for Arg in the SDH3 "Sx_2HR" motif and histidines as heme ligands in SDH3 and SDH4 (Yankovskaya et al., 2003; Sun et al., 2005). It has been suggested that the role of a heme ligand in helix II (His84 in *E. coli* SDH3) could be replaced by a nearby histidine in the quinone-binding motif "Sx_2HR" in helix I (Maklashina et al., 2001). In SDH4 from *Saccharomyces cerevisiae* strain S288C (NP_010463) and rice (NP_001045324), the heme ligand His is substituted by Tyr and Gln, respectively. In catalase (Fita and Rossmann, 1985)

Fig. 7. Sequence alignment of subunit *b* (ATP4) of protist ATP synthase. Sequences used (GenBank accession No.) are *P. falciparum* (XP_001349752), *P. vivax* (XP_001613405), *P. berghei* (XP_680022), *P. c. chabaudi* (XP_743670), *Paramecium tetraurelia* (XP_001429993), *T. brucei* (XP_844845), *R. americana* (NP_044805), *Hemiselmis andersenii* (YP_001874763), *D. discoideum* (YP_001604088), *Phytophthora brassicae* (ES285372), *C. merolae* (NP_059355), *S. cerevisiae* (NP_015247), *Marchantia polymorpha* (NP_054459), *A. thaliana* (NP_085524), *D. melanogaster* (Q94516), *N. vectensis* (XP_001635800), *H. sapiens* (NP_001679), *Bradyrhizobium japonicum* (NP_767825), and *E. coli* (NP_418192). Domain structures shown are those proposed for *E. coli* AtpF (Dunn et al., 2000). Transmembrane helices predicted by TMHMM are indicated in *blue* and conserved residues are shown in *red*.

and other hemoproteins Tyr can coordinate the heme and the His-to-Tyr mutant of the yeast SDH3 "YHx$_{10}$D" motif retained half of the enzyme activity and heme content (Oyedotun and Lemire, 1999). In contrast to rhodoquinol–fumarate reductase (type C FRD) from parasitic nematodes (Saruta et al., 1995), menaquinol–fumarate reductase (type D FRD) from *E. coli* lacks heme *b* although membrane anchor subunits FrdC and FrdD have His and Cys, respectively, at the equivalent position of His84 and His71 of *E. coli* SdhC and SdhD, respectively (Hägerhäll, 1997; Cecchini, 2003). Depending on host environments, like *E. coli* FRD, *Plasmodium* Complex II may be able to catalyze both succinate oxidation and fumarate reduction despite *Plasmodium* mitochondria do not have low potential quinones. The presence or absence of the bound protoheme IX in *Plasmodium* Complex II and its enzymatic properties must be tested in future studies using the purified enzyme.

3.4. Membrane anchor subunits of Plasmodium ATP synthase

For a long time, it has been assumed that *Plasmodium* mitochondria cannot carry out oxidative phosphorylation (Fry and

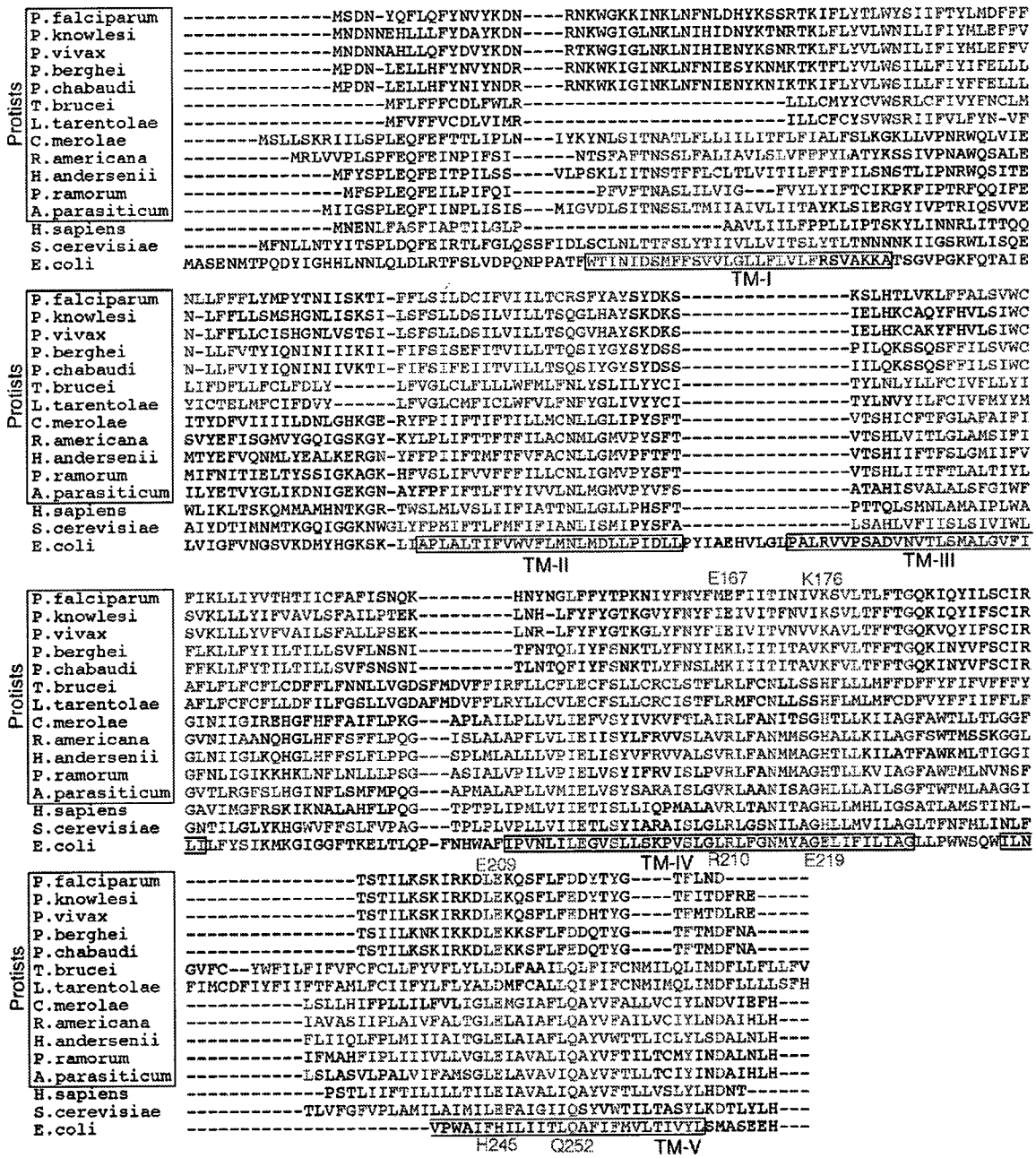

Fig. 8. Sequence alignment of subunit *a* (ATP6) of protist ATP synthase. Sequences used (GenBank accession No.) are *P. falciparum* (XP_001347344), *P. knowlesi* (CAQ39459), *P. vivax* (XP_001614365), *P. berghei* (XP_676120), *P. chabaudi* (XP_745940), *T. brucei* (AAA97428), *L. tarentolae* (AAA96695), *C. merolae* (NP_059364), *R. americana* (NP_044804), *H. andersenii* (YP_001874775), *D. discoideum* (NP_050086), *Phytophthora ramorum* (YP_001165346), *Amoebidium parasiticum* (AAN04079), *H. sapiens* (NP_536848), *S. cerevisiae* (CAA24054), and *E. coli* (NP_418194). Transmembrane helices (TM) predicted by TMHMM are indicated in *blue* and those proposed for *E. coli* AtpB (Moore et al., 2008) are boxed. Conserved amino acid residues in TM-IV and -V are shown in *red*.

Beesley, 1991) because of the apparent lack of transmembrane subunits *a* and *b* of the H^+-translocating F_oF_1-ATP synthase (Carlton et al., 2002; Gardner et al., 2002). However, oxidative phosphorylation in rodent malaria mitochondria (Uyemura et al., 2000, 2004) supports the presence of subunits *a* an *b* of the F_o subcomplex, which serve as the stator in the rotary mechanism (Noji et al., 1997; Fillingame et al., 2000) (Fig. 2), in *Plasmodium* ATP synthase.

Subunits *a* and *b* of protist ATP synthase are also highly divergent from bacterial and eukaryotic counterparts and are frequently not anotated in the database (Seeber et al., 2008). In mitochondrial genomes of land plants and certain protists, ORFs *ymf19* (*orfB*) and *ymf39* are conserved. Based on the sequence similarity and of mass spectrometric analysis, *Ymf19/OrfB* was assigned as subunit ATP8 (A6L) of the sunflower ATP synthase (Sabar et al., 2003). By protein sequencing and mass spectrometric analysis, Ymf39 was assigned as subunit *b* (ATP4 in mitochondria, AtpF in bacteria) in the jakobid *Seculamonas ecuadoriensis* (Burger et al., 2003), and the kinetoplastids *Crithidia fasciculata* (Speijer et al., 1997) and *Leishmania tarentolae* (Nelson et al., 2004). Based on peptide sequences of the *C. fasciculate* ATP synthase subunits, Allen et al. (2004) identified seven subunits of *Trypanosoma brucei* ATP synthase. By using these protist sequences as queries, we identified candidates for 10 subunits of *Plasmodium* ATP synthase with the current database (Table 1). In the mitochondrial ATP synthase, subunits *b* and ε of bacterial enzymes are split to subunits *b* and *d* and subunits δ_m and ε_m, respectively. We noticed that ATP16 (ε, δ_m) was mislabeled as ATP15 (ε_m) in *T. brucei* ATP synthase (Allen et al., 2004). Trypanosomatid p18 has been assigned as subunit *b* in previous studies (Nelson et al., 2004; Zíková et al., 2009). It is a hydrophilic nuclear gene product and our sequence analysis indicates that trypanosomatid and euglenid p18s are more closely related to subunit *d* (ATP7) (Devenish et al., 2000) (Fig. 6). As discussed by Burger et al. (2003), subunit *b* is rather featureless except for the locations of its transmembrane helices in the *N*-terminal region (Dunn et al., 2000) and there is no strictly conserved residue throughout species (Fig. 7).

Since the *C. fasciculate* band 3 homolog has four putative transmembrane helices, we tentatively assigned band 3 as subunit *a* (ATP6, AtpB) among four unassigned subunits of *T. brucei* ATP synthase (Allen et al., 2004). Using the *T. brucei* sequence as a query, we identified *Plasmodium* subunit *a* (Fig. 8). The sequence identities of *P. falciparum* subunit *a* with the *E. coli* AtpB (Fig. 4C) and *H. sapiens* ATP6 are 12.9% and 18.8%, respectively. TM-I of *Plasmodium* and *Trypanosoma* spp. showed a high sequence similarity and TM-IV and TM-V are conserved throughout species. Arg210 in transmembrane helix IV (*E. coli* AtpB numbering), which is essential for the proton translocation through the F_o subcomplex (Valiyaveetil and Fillingame, 1977; Fillingame et al., 2000; Moore et al., 2008), is substituted by Glu and Lys in human and rodent malaria parasites, respectively (Figs. 4D and 8). In *E. coli*, second site suppressor mutations of Arg210Gln in TM-IV have been identified as Gln252Arg and Gln252Lys in TM-V (Hatch et al., 1995; Ishmukhametov et al., 2008), indicating close proximity of these conserved residues. Notably, a pair of residues at positions 219 and 245 of *E. coli* subunit *a* are interchanged in mitochondria and the *E. coli* double mutant Glu219His/His245Glu was a slightly functional (Cain and Simoni, 1988). In the malaria parasites, Gln252 is replaced by Asp or Glu and Glu219 and His245 by Lys and Glu, respectively. Despite a lack of Arg210, a set of amino acid substitutions would make the *Plasmodium* subunit *a* functional.

In conclusion, here we identified candidates for six F_1 subunits [α, β, γ, δ (ATP5, OSCP), δ_m, and ε_m] and four F_o subunits (*a–d*) in *Plasmodium* spp (Table 1). Thus, the *Plasmodium* ATP synthase contains all eight subunits of the *E. coli* ATP synthase ($\alpha_3\beta_3\gamma_1\delta_1\varepsilon$-(=$\delta_m$ *plus* ε_m)$_1a_1b$(=*b plus d*)$_1c_{10?}$) and could carry out a rotary mechanism for ATP synthesis (Noji et al., 1997; Fillingame et al., 2000). Phylogenetic analysis showed that, in contrast to soluble catalytic subunit β (not shown), all three membrane anchor subunits, *a*, *b* (Fig. 9) and *c* (not shown), of *Plasmodium* and *Trypanosoma* spp. are divergent from their mitochondrial orthologs. Diversity in membrane anchors of parasitic protist mitochondrial ATP synthase suggests the plasticity in their structures even though they are essential for oxidative phosphorylation. Such variations may modulate or attenuate the function in host environments.

4. Conclusion and perspectives

We identified candidates for the membrane anchors of *Plasmodium* Complex II based on the presence of the structural fingerprints and showed sequence divergence from the eukaryotic orthologs. ATPase subunits *a* and *b* of *Plasmodium* were identified based on proteomics data of other protists, and again we found high sequence divergence in the membrane anchors. Our studies

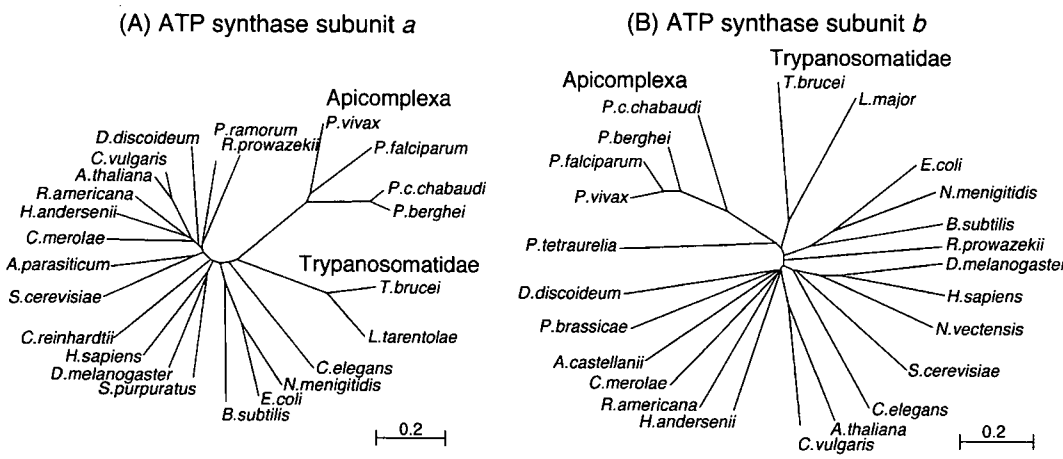

Fig. 9. Unrooted phylogenetic trees for subunit *a* (A) and *b* (B) of F-type ATP synthase. Subunits *a* and *b* sequences (GenBank accession Nos.) used are *D. melanogaster* (NP_008281, Q94516), *C. elegans* (NP_006956, NP_497938), *Strongylocentrotus purpuratus* (NP_006971, not available), *A. thaliana* (NP_085569, NP_085524), *Chara vulgaris* (NP_943689, NP_943702), *Chlamydomonas reinhardtii* (XP_001689492, not available), *L. major* (not available, XP_001686628), *Acanthamoeba castellanii* (not available, NP_042558), *R. prowazekii* (NP_220417, NP_220414), *Neisseria meningiditis* (NP_274934, NP_274932), and *Bacillus subtilis* (NP_391568, NP_391566). All other sequences were described in the legends to Figs. 7 and 8. The mitochondrial genomes encode eukaryotic subunits *a* except *C. reinhardtii* and *Plasmodium* spp. and subunit *b* of plants and some protists (*D. discoideum*, *C. merolae*, *R. americana*, and *H. andersenii*).

suggest that *Plasmodium* mitochondria possess all catalytic subunits for Complex II and ATP synthase (Table 1) and are fully capable of oxidative phosphorylation. Our approach is applicable to other membrane proteins although it is rather low throughput. Our assignments should help in understanding parasite energy metabolism.

Recently, diarylquinoline, a new tuberculosis-specific agent, has been shown to bind subunit *c* of ATP synthase (Andries et al., 2005). *Plasmodium* Complex II and ATP synthase could be pathogen-specific targets for new antimalarial agents, because of sequence divergence in membrane anchor subunits. In addition, alternative respiratory enzymes like NDH2 and malate:quinone oxidoreductase (MQO) are absent in mammalian mitochondria and are also promising targets. Since inhibitors for NDH2 are rare and mostly nonspecific (Kerscher, 2000), we screened natural antibiotics and identified gramicidin S and scopafungin as new inhibitors (Mogi et al., 2009). (Saleh et al., 2007) found that 1-hydroxy-2-dodecyl-4(1*H*)quinolone (HDQ), a potent inhibitor for yeast NDH2 (Eschemann et al., 2005), can act as an antimalarial. Even though our compounds were less effective on the *Plasmodium* enzyme than on bacterial enzymes, they may still serve as antimalarials. Such continuing efforts on the screening of natural and synthetic compounds could identify novel and potent drugs against malaria.

Acknowledgements

This study was supported by a grant-in-aid for scientific research (20570124 to TM) and Creative Scientific Research (18GS0314 to KK) from the Japan Society for the Promotion of Science, and a grant-in-aid for scientific research on Priority Areas (18073004 to KK) from the Ministry of Education, Culture, Sports, Science and Technology, Japan. We would like to thank Dr. B. Lemire (University of Alberta), Dr. G. Burger (University of Montreal), and Dr. S. Sato (National Institute for Medical Research, UK) for critical reading of the manuscript, Dr. M. Llinás (Princeton University), Dr. L. Lasonder, and Dr. H.E. Stunnenberg (Radboud University Nijmegen) for the use of their unpublished results.

References

Allen, J.W.A., Ginger, M.L., Ferguson, S.J., 2004. Maturation of the unusual single-cysteine (XXXCH) mitochondrial *c*-type cytochromes found in trypanosomatids must occur through a novel biogenesis pathway. Biochem. J. 383, 537–542.

Andries, K., Verhasselt, P., Guillemont, J., Göhlmann, H.W.H., Neefs, J.M., Winkler, H., Gestel, J.V., Timmerman, P., Zhu, M., Lee, E., Williams, P., de Chaffoy, D., Huitric, E., Hoffner, S., Cambau, E., Truffot-Pernot, C., Lounis, N., Jarlier, V., 2005. A diarylquinoline drug active on the ATP synthase of *Mycobacterium tuberculosis*. Science 307, 223–227.

Biagini, G.A., Viriyavejakul, P., O'Neill, P.M., Bray, P.G., Ward, S.A., 2006. Functional characterization and target validation of alternative Complex I of *Plasmodium falciparum* mitochondria. Antimicrob. Agents Chemother. 50, 1841–1851.

Burger, G., Lang, B.F., Braun, H.-P., Marx, S., 2003. The enigmatic mitochondrial ORF *ymf39* codes for ATP synthase chain *b*. Nucleic Acids Res. 31, 2353–2360.

Cain, B.D., Simoni, R.D., 1988. Interaction between Glu-219 and His-245 within the *a* subunit of F_1F_0-ATPase in *Escherichia coli*. J. Biol. Chem. 263, 6606–6612.

Carlton, J.M., Angiuoli, S.V., Suh, B.B., Kooij, T.W., Pertea, M., Silva, J.C., Ermolaeva, M.D., Allen, J.E., Selengut, J.D., Koo, H.L., Peterson, J.D., Pop, M., Kosack, D.S., Shumway, M.F., Bidwell, S.L., Shallom, S.J., van Aken, S.E., Riedmuller, S.B., Feldblyum, T.V., Cho, J.K., Quackenbush, J., Sedegah, M., Shoaibi, A., Cummings, L.M., Florensk, L., Yatesk, J.R., Raine, J.D., Sinden, R.E., Harris, M.A., Cunningham, D.A., Preiser, P.R., Bergman, L.W., Vaidya, A.B., van Lin, L.H., Janse, C.J., Waters, A.P., Smith, H.O., White, O.R., Salzberg, S.L., Venter, J.C., Fraser, C.M., Hoffman, S.L., Gardner, M.J., Carucci, D.J., 2002. Genome sequence and comparative analysis of the model rodent malaria parasite *Plasmodium yoelii yoelii*. Nature 419, 512–519.

Cecchini, G., 2003. Function and structure of Complex II of the respiratory chain. Annu. Rev. Biochem. 72, 77–109.

Daily, J.P., Scanfeld, D., Pochet, N., Roch, K.L., Plouffe, D., Kamel, M., Sarr, O., Mboup, S., Ndir, O., Wypij, D., Lavasseur, K., Thomas, E., Tamayo, P., Dong, C., Zhou, Y., Lander, E.S., Ndiaye, D., Wirth, D., Winzeler, E.A., Mesirov, J.P., Regev, A., 2007. Distinct physiological states of *Plasmodium falciparum* in malaria-infected patients. Nature 450, 1091–1095.

Devenish, R.J., Prescott, M., Roucou, X., Nagley, P., 2000. Insights into ATP synthase assembly and function through the molecular genetic manipulation of subunits of the yeast mitochondrial enzyme complex. Biochim. Biophys. Acta 1458, 428–442.

Dunn, S.D., McLachlin, D.T., Revington, M., 2000. The second stalk of *Escherichia coli* ATP synthase. Biochim. Biophys. Acta 1468, 356–363.

Eschemann, A., Galkin, A., Oettmeier, W., Brandt, U., Kerscher, S., 2005. HDQ (1-hydroxy-2-dodecyl-4(1*H*)quinolone), a high affinity inhibitor for mitochondrial alternative NADH dehydrogenase: evidence for a ping-pong mechanism. J. Biol. Chem. 280, 3138–3142.

Fillingame, R.H., Jiang, W., Dimitriev, O.Y., 2000. Coupling of H^+ transport to rotary catalysis in F-type ATP synthases: structure and organization of the transmembrane rotary motor. J. Exp. Biol. 203, 9–17.

Fita, I., Rossmann, M.G., 1985. The active center of catalase. J. Mol. Biol. 185, 21–37.

Foth, B.J., Stimmler, L.M., Handman, E., Crabb, B.S., Hodder, A.N., McFadden, G.I., 2005. The malaria parasite *Plasmodium falciparum* has only one pyruvate dehydrogenase complex, which is located in the apicoplast. Mol. Microbiol. 55, 39–53.

Fry, M., Webb, E., Pudney, M., 1990. Effect of mitochondrial inhibitors on adenosine triphosphate levels in *Plasmodium falciparum*. Comp. Biochem. Physiol. B 96, 775–782.

Fry, M., Beesley, J.E., 1991. Mitochondria of mammalian *Plasmodium* spp. Parasitology 102, 17–26.

Gardner, M.J., Hall, N., Fung, E., White, O., Berriman, M., Hyman, R.W., Carlton, J.M., Pain, A., Nelson, K.E., Bowman, S., Paulsen, I.T., James, K., Eisen, J.A., Rutherford, K., Salzberg, S.L., Craig, A., Kyes, S., Chan, M.S., Nene, V., Shallom, S.J., Suh, B., Peterson, J., Angiuoli, S., Pertea, M., Allen, J., Selengut, J., Haft, D., Mather, M.W., Vaidya, A.B., Martin, D.M., Fairlamb, A.H., Fraunholz, M.J., Roos, D.S., Ralph, S.A., McFadden, G.I., Cummings, L.M., Subramanian, G.M., Mungall, C., Venter, J.C., Carucci, D.J., Hoffman, S.L., Newbold, C., Davis, R.W., Fraser, C.M., Barrell, B., 2002. Genome sequence of the human malaria parasite *Plasmodium falciparum*. Nature 419, 498–511.

Hägerhäll, C., 1997. Succinate: quinone oxidoreductases. Variations on a conserved theme. Biochim. Biophys. Acta 1320, 107–141.

Hatch, L.P., Cox, G.B., Howitt, S.M., 1995. The essential arginine residue at position 210 in the *a* subunit of the *Escherichia coli* ATP synthase can be transferred to position 252 with partial retention of activity. J. Biol. Chem. 270, 29407–29412.

Henn, M.W., Schopf, R., Maier, W.A., Seitz, H.M., 1998. The amino acid composition of *Anopheles stephensi* (Diptera: Culicidae) infected with *Nosema algerae* (Microsporida: Nosematidae). J. Invertebr. Pathol. 71, 42–47.

Horsefield, R., Yankovskaya, V., Sexton, G., Whittingham, W., Shiomi, K., Ōmura, S., Byrne, B., Cecchini, G., Iwata, S., 2006. Structural and computational analysis of the quinone-binding site of Complex II (succinate–ubiquinone oxidoreductase). A mechanism of electron transfer and proton conduction during ubiquinone reeuction. J. Biol. Chem. 281, 7309–7316.

Hurles, M., 2004. Gene duplication: the genomic trade in spare parts. PLoS Biol. 2, 0900–0904.

Hyde, J.E., 2005. Drug-resistant malaria. Trends Parasitol. 21, 494–498.

Ishmukhametov, R.R., Pond, J.B., Al-Huqail, A., Galkin, M.A., Vik, S.B., 2008. ATP synthesis without R210 of subunit *a* in the *Escherichia coli* ATP synthase. Biochim. Biophys. Acta 1777, 32–38.

Kawahara, K., Mogi, T., Tanaka, T.Q., Hata, M., Miyoshi, H., Kita, K., 2009. Mitochondrial dehydrogenases in the aerobic respiratory chain of the rodent malaria parasite *Plasmodium yoelii yoelii*. J. Biochem. 145, 229–237.

Kerscher, S.J., 2000. Diversity and origin of alternative NADH:ubiquinone oxidoreductase. Biochim. Biophys. Acta 1459, 274–283.

Larkin, M.A., Blackshields, G., Brown, N.P., Chenna, R., McGettigan, P.A., McWilliam, H., Valentin, F., Wallace, I.M., Wilm, A., Lopez, R., Thompson, J.D., Gibson, T.J., Higgins, D.G., 2007. ClustalW2 and ClustalX version 2. Bioinformatics 23, 2947–2948.

Lasonder, E., Janse, C.J., van Gemert, G., Mair, G.R., Vermunt, A.M.W., Douradinha, B.G., van Noort, V., Huynen, M.A., Luty, A.J.F., Kroeze, H., Khan, S.M., Sauerwein, R.W., Waters, A.P., Mann, M., Stunnenberg, H.G., 2008. Proteomic profiling of *Plasmodium* sporozoite maturation identifies new proteins essential for parasite development and infectivity. PLoS Pathogens 4, e1000195.

Maklashina, E., Rothery, R.A., Weiner, J.H., Cecchini, G., 2001. Retention of heme in axial ligand mutants of succinate–ubiquinone oxidoreductase (Complex II) from *Escherichia coli*. J. Biol. Chem. 276, 18968–18976.

Mi-Ichi, F., Miyadera, H., Kobayashi, T., Takamiya, S., Waki, S., Iwata, S., Shibata, S., Kita, K., 2005. Parasite mitochondria as a target of chemotherapy: inhibitory effect of licochalcone A on the *Plasmodium falciparum* respiratory chain. Ann. NY. Acad. Sci. 1056, 46–54.

Mogi, T., Matsushita, K., Miyoshi, H., Ui, H., Shiomi, K., Ōmura, S., Kita, K., 2009. Identification of new inhibitors for alternative NADH dehydrogenase (NDH-II). FEMS Microbiol. Lett. 291, 157–161.

Moore, K.J., Angevine, C.M., Vincent, O.D., Schwem, B.E., Fillingame, R.H., 2008. The cytoplasmic loops of subunit a of *Escherichia coli* ATP synthase may participate in the proton translocation mechanism. J. Biol. Chem. 283, 13044–13052.

Morales, J., Mogi, T., Mineki, S., Takashima, E., Mineki, R., Hirawake, H., Sakamoto, K., Ōmura, S., Kita, K., 2009. Novel mitochondrial Complex II isolated from *Trypanosoma cruzi* is composed of twelve peptides including a heterodimeric Ip subunit. J. Biol. Chem. 284, 7255–7263.

Nelson, R.E., Aphasizheva, I., Falick, A.M., Nebohacova, M., Simpson, L., 2004. The I-complex in *Leishmania tarentolae* is an uniquely-structured F_1-ATPase. Mol. Biochem. Parasitol. 135, 221–224.

Noji, H., Yasuda, R., Yoshida, M., Kinosita, K., 1997. Direct observation of the rotation of F_1-ATPase. Nature 386, 299–302.

Oyedotun, K.S., Lemire, B.D., 1999. The *Saccharomyces cerevisiae* succinate–ubiquinone oxidoreductase. Identification of Sdh3p amino acid residues involved in ubiquinone binding. J. Biol. Chem. 274, 23956–23962.

Oyedotun, K.S., Sit, C.S., Lemire, B.D., 2007. The *Saccharomyces cerevisiae* succinate dehydrogenase does not require heme for ubiquinone reduction. Biochim. Biophys. Acta 1767, 1436–1445.

Painter, H.J., Morrisey, J.M., Mather, M.W., Vaidya, A.B., 2007. Specific role of mitochondrial electron transport in blood-stage *Plasmodium falciparum*. Nature 446, 88–91.

Sabar, M., Gagliardi, D., Balk, J., Leaver, C., 2003. ORFB is a subunit of F_1F_o-ATP synthase: insight into the basis of cytoplasmic male sterility in sunflower. EMBO Rep. 4, 381–386.

Saleh, A., Friesen, J., Baumeister, S., Gross, G., Bohne, W., 2007. Growth inhibition of *Toxoplasma gondii* and *Plasmodium falciparum* by nanomolar concentrations of 1-hydroxy-2-dodecyl-4(1*H*)quinolone, a high-affinity inhibitor of alternative (type II) NADH dehydrogenases. Antimicrob. Agents Chemother. 51, 1217–1222.

Saruta, F., Kuramochi, T., Nakamura, K., Takamiya, S., Yu, Y., Aoki, T., Sekimizu, K., Kojima, S., Kita, K., 1995. Stage-specific isoforms of complex II (succinate–ubiquinone oxidoreductase) in mitochondria from the parasitic nematode, *Ascaris suum*. J. Biol. Chem. 270, 928–932.

Seeber, F., Limenitakis, J., Soldati-Favre, D., 2008. Apicomplexan mitochondrial metabolism: a story of gains, losses and retentions. Trends Parasitol. 24, 468–478.

Sherman, I.W., 1998. Carbohydrate metabolism of asexual stages. In: Sherman, I.W. (Ed.), Malaria, Parasite Biology, Pathogenesis and Protection. ASM Press, Washington, DC, pp. 135–143.

Speijer, D., Breek, C.K., Muijsers, A.O., Hartog, A.F., Berden, J.A., Albracht, S.P., Samyn, B., van Beeumen, J., Benne, R., 1997. Characterization of the respiratory chain from cultured *Crithidia fasciculate*. Mol. Biochem. Parasitol. 85, 171–186.

Srivastava, I.K., Rottenberg, H., Vaidya, A.B., 1997. Atovaquone, a broad spectrum antiparasitic drug, collapses mitochondrial membrane potential in malarial parasite. J. Biol. Chem. 272, 3961–3966.

Sun, F., Huo, X., Zhai, Y., Wang, A., Xu, J., Su, D., Bartlam, M., Rao, Z., 2005. Crystal structure of mitochondrial respiratory membrane protein complex II. Cell 121, 1043–1057.

Suraveratum, N., Krungkrai, S.R., Leangaramgul, P., Prapunwattana, P., Krungkrai, J., 2000. Purification and characterization of *Plasmodium falciparum* succinate dehydrogenase. Mol. Biochem. Parasitol. 105, 215–222.

Takashima, E., Takamiya, S., Takeo, S., Mi-ichia, F., Amino, H., Kita, K., 2001. Isolation of mitochondria from *Plasmodium falciparum* showing dihydroorotate dependent respiration. Parasitol. Int. 50, 273–278.

Takeo, S., Kokaze, A., Ng, C.S., Mizuchi, D., Watanabe, J.I., Tanabe, K., Kojima, S., Kita, K., 2000. Succinate dehydrogenase in *Plasmodium falciparum* mitochondria: molecular characterization of the *SDHA* and *SDHB* genes for the catalytic subunits, the flavoprotein (Fp) and iron–sulfur (Ip) subunits. Mol. Biochem. Parasitol. 107, 191–205.

Tran, Q.M., Rothery, R.A., Maklashina, E., Cecchini, G., Weiner, J.H., 2007. *Escherichia coli* succinate dehydrogenase variant lacking the heme *b*. Proc. Natl. Acad. Sci. USA 104, 18007–18012.

Uyemura, S.A., Luo, S., Moreno, S.N.J., Docampo, R., 2000. Oxidative phosphorylation, Ca^{2+} transport, and fatty acid-induced uncoupling in malaria parasites mitochondria. J. Biol. Chem. 275, 9709–9715.

Uyemura, S.A., Luo, S., Vieira, M., Moreno, S.N., Docampo, R., 2004. Oxidative phosphorylation and rotenone-insensitive malate- and NADH-quinone oxidoreductases in *Plasmodium yoelii yoelii* mitochondria *in situ*. J. Biol. Chem. 279, 385–393.

Vaidya, A.B., Mather, M.W.A., 2005. Post-genomic view of the mitochondrion in malaria parasites. Curr. Top. Microbiol. Immunol. 295, 233–250.

Valiyaveetil, F.I., Fillingame, R.H., 1977. On the role of Arg-210 and Glu-219 of subunit *a* in proton translocation by the *Escherichia coli* F_oF_1-ATP synthase. J. Biol. Chem. 272, 32635–32641.

van Dooren, G.G., Stimmler, L.M., McFadden, G.I., 2006. Metabolic maps and functions of the *Plasmodium* mitochondrion. FEMS Microbiol. Rev. 30, 596–630.

Vaughan, A., Chiu, S., Ramasamy, G., Li, L., Gardner, M.J., Tarun, A.S., Kappe, S.H.I., Peng, X., 2008. Assessment and improvement of the *Plasmodium yoelii yoelii* genome annotation through comparative analysis. ISMB 24, i383–i389.

Yang, X., Yu, L., He, D., Yu, C.A., 1998. The quinone-binding site in succinate–ubiquinone reductase from *Escherichia coli*. Quinone-binding domain and amino acid residues involved in quinone binding. J. Biol. Chem. 273, 31916–31923.

Yankovskaya, V., Horsefield, R., Tornroth, S., Luna-Chavez, C., Miyoshi, H., Leger, C., Byrne, B., Cecchini, G., Iwata, S., 2003. Architecture of succinate dehydrogenase and reactive oxygen species generation. Science 299, 700–704.

Zíková, A., Schnaufer, A., Dalley, R.A., Panigrahi, A.K., Stuart, K.D., 2009. The F_oF_1-ATP synthase complex contains novel subunits and is essential for procyclic *Trypanosoma brucei*. PLoS Pathogens 5, e1000436.

Acta Crystallographica Section F
Structural Biology and Crystallization Communications
ISSN 1744-3091

Crystallization and preliminary X-ray analysis of aspartate transcarbamoylase from the parasitic protist *Trypanosoma cruzi*

Kazuaki Matoba,[a] Takeshi Nara,[b] Takashi Aoki,[b] Teruki Honma,[c] Akiko Tanaka,[c] Masayuki Inoue,[d] Shigeru Matsuoka,[d] Daniel Ken Inaoka,[e] Kiyoshi Kita[e] and Shigeharu Harada[a]*

[a]Department of Applied Biology, Graduate School of Science and Technology, Kyoto Institute of Technology, Kyoto 606-8585, Japan, [b]Department of Molecular and Cellular Parasitology, Juntendo University School of Medicine, Tokyo 113-8421, Japan, [c]Systems and Structural Biology Center, RIKEN, Tsurumi, Yokohama 230-0045, Japan, [d]Graduate School of Pharmaceutical Sciences, The University of Tokyo, Tokyo 113-0033, Japan, and [e]Department of Biomedical Chemistry, Graduate School of Medicine, The University of Tokyo, Tokyo 113-0033, Japan

Correspondence e-mail: harada@kit.ac.jp

Received 23 April 2009
Accepted 12 August 2009

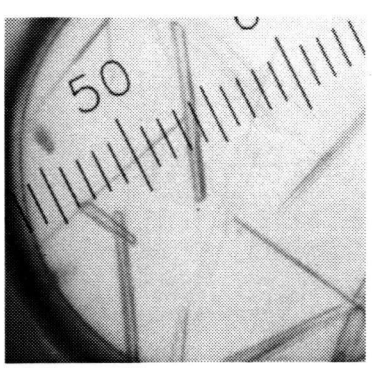

Aspartate transcarbamoylase (ATCase), the second enzyme of the *de novo* pyrimidine-biosynthetic pathway, catalyzes the production of carbamoyl aspartate from carbamoyl phosphate and L-aspartate. In contrast to *Escherichia coli* ATCase and eukaryotic CAD multifunctional fusion enzymes, *Trypanosoma cruzi* ATCase lacks regulatory subunits and is not part of the multifunctional fusion enzyme. Recombinant *T. cruzi* ATCase expressed in *E. coli* was purified and crystallized in a ligand-free form and in a complex with carbamoyl phosphate at 277 K by the sitting-drop vapour-diffusion technique using polyethylene glycol 3350 as a precipitant. Ligand-free crystals (space group $P1$, unit-cell parameters a = 78.42, b = 79.28, c = 92.02 Å, α = 69.56, β = 82.90, γ = 63.25°) diffracted X-rays to 2.8 Å resolution, while those cocrystallized with carbamoyl phosphate (space group $P2_1$, unit-cell parameters a = 88.41, b = 158.38, c = 89.00 Å, β = 119.66°) diffracted to 1.6 Å resolution. The presence of two homotrimers in the asymmetric unit (38 kDa × 6) gives V_M values of 2.3 and 2.5 Å^3 Da^{-1} for the $P1$ and $P2_1$ crystal forms, respectively.

1. Introduction

Chagas disease is a serious tropical disease that is endemic in Central and South America, affecting approximately 16–18 million people in these areas. The causative agent is a flagellate parasitic protist, *Trypanosoma cruzi*, which is transmitted by blood-feeding reduviid bugs. Manifestations of Chagas disease include severe cardiomyopathy, digestive injuries and neural disorders resulting from gradual tissue destruction caused by the parasite. Because nifurtimox and benznidazole, which are the currently used drugs for the treatment of Chagas disease, are toxic and ineffective in the chronic phase, the development of new chemotherapeutic drugs is urgently required (Urbina, 2002).

Pyrimidine biosynthesis is indispensable to all organisms and is achieved *via* the *de novo* and/or salvage pathways. *T. cruzi* possesses both pathways and their balance varies at different developmental stages of the parasite. Since the amastigote stage essentially relies on the *de novo* pathway (Gutteridge & Gaborak, 1979), in which uridine 5′-monophosphate is produced through a series of six enzymatic reactions, the enzymes of the *de novo* pathway therefore provide a greater potential as the primary targets of chemotherapy (Urbina & Docampo, 2003).

Aspartate transcarbamoylase (ATCase; EC 2.1.3.2), the second enzyme of the *de novo* pyrimidine-biosynthetic pathway, catalyzes the production of carbamoyl aspartate from carbamoyl phosphate (CP) and L-aspartate. *Escherichia coli* ATCase is a well known allosteric enzyme and is comprised of catalytic and regulatory subunits, the latter of which carries the binding site of the feedback inhibitor cytidine 5′-triphosphate (CTP; Gerhart & Pardee, 1964; Gerhart & Schachman, 1965; Shepherdson & Pardee, 1960). X-ray structural analysis of the *E. coli* enzyme demonstrated that the enzyme is composed of two trimers of the catalytic subunit (c) and three dimers of the regulatory subunit (r) to form a $(c_3)_2(r_2)_3$ quaternary structure (Krause *et al.*, 1985; Wiley *et al.*, 1972; Wiley & Lipscomb, 1968). ATCases from different strains of *Yersinia enterocolitica* and *Y. enterocolitica*-like organisms also exhibit the $(c_3)_2(r_2)_3$ structure but are sensitive to feedback inhibition by different

pyrimidine nucleotides (Foltermann *et al.*, 1981). *Bacillus subtilis* ATCase lacks the regulatory subunits (Stevens *et al.*, 1991) and in the hyperthermophile *Aquifex aeolicus* six ATCase chains noncovalently associate with six molecules of dihydroorotase (DHO), the third enzyme of the pyrimidine-biosynthetic pathway, to form a dodecamer (Zhang *et al.*, 2009).

On the other hand, eukaryotic ATCases from animals, fungi and Amoebozoa fuse with carbamoyl-phosphate synthetase II (CPS II; the first enzyme of the *de novo* pathway) and DHO to form a multifunctional fusion protein called CAD (Coleman *et al.*, 1977; Freund & Jarry, 1987; Simmer *et al.*, 1989; Souciet *et al.*, 1987), whose feedback inhibitor (CTP) binding site is located in the CPS II domain (Liu *et al.*, 1994). In contrast, *T. cruzi* ATCase (TcATCase), together with the ATCases from plants and other protists, is not part of the CAD multifunctional enzyme and is virtually insensitive to feedback inhibition by pyrimidine nucleotides (Aoki & Oya, 1987) since the enzyme lacks the regulatory subunit (El-Sayed *et al.*, 2005; Gao *et al.*, 1999). In addition, *N*-(phosphonoacetyl)-L-aspartate (PALA), a specific inhibitor of bacterial and mammalian ATCases (Aoki, 1994), only weakly inhibits TcATCase. Thus, structure determination of TcATCase, as well as of the other *de novo* pyrimidine-biosynthetic enzymes of *T. cruzi*, is considered to be crucial for the rational design of chemotherapeutic agents against Chagas disease.

Currently, the crystal structures of bacterial ATCases from *Escherichia coli* (Honzatko *et al.*, 1982), *Bacillus subtilis* (Stevens *et al.*, 1991), *Pyrococcus abyssi* (Van Boxstael *et al.*, 2003), *Sulfolobus acidocaldarius*, *Moritella profunda* (De Vos *et al.*, 2004, 2007) and *Methanococcus jannaschii* (Vitali & Colaneri, 2008), and of the *A. aeolicus* ATCase–DHO complex (Zhang *et al.*, 2009) have been reported. In the present study, we report the expression, purification, crystallization and preliminary X-ray analysis of TcATCase. This is the first crystallization report of an eukaryotic ATCase.

2. Materials and methods

2.1. Preparation of *T. cruzi* ATCase

The *T. cruzi* ATCase genes were previously cloned by screening the total DNA library of *T. cruzi* Tulahuen strain (Nara *et al.*, 2003). *T. cruzi* Tulahuen possesses three copies of the ATCase gene (*tcact1*, *tcact2* and *tcact3*, with GenBank accession Nos. AB074138, AB074139 and AB074140, respectively) and *tcact2* was selected for expression. The open reading frame of *tcact2* was amplified by PCR using 5′-CGGGATCCATGTTGGAACTGCCGCCAG-3′ and 5′-CGGG-ATCCTCACGCCAAAACGCTCCAC-3′ as the forward and reverse primers, respectively, and then subcloned into the bacterial expression vector pET14b (Novagen, EMD Biosciences Inc., Madison, Wisconsin, USA). The recombinant plasmid was introduced into *E. coli* BL21 (DE3) pLysS (Novagen). The transformant was grown in 1000 ml Luria–Bertani medium containing 50 μg ml^{-1} carbenicillin at 310 K until the absorbance at 600 nm (A_{600}) reached about 0.6. Expression of the recombinant His_6-tagged TcATCase was induced with 1 m*M* isopropyl β-D-1-thiogalactopyranoside at 310 K for 2 h. The cells were harvested by centrifugation at 5000*g* for 10 min and suspended in 20 ml lysis buffer (20 m*M* Tris–HCl pH 8.0, 0.5 *M* NaCl, 40 m*M* imidazole). After disruption of the cells by sonication, the lysate was centrifuged at 15 000*g* at 277 K for 20 min. The supernatant containing the His_6-tagged TcATCase was filtrated with a 0.22 μm pore-size filter and loaded onto a His-Trap FF column (1 ml bed volume; GE Healthcare) pre-equilibrated with lysis buffer. The column was then washed with 20 ml lysis buffer and the bound His_6-tagged TcATCase was eluted from the column with lysis buffer containing 500 m*M* imidazole. The fractions containing TcATCase were pooled and the buffer was exchanged to 20 m*M* Tris–HCl pH 7.4 using a PD-10 desalting column (GE Healthcare); they were then concentrated to 10 mg ml^{-1} with a centrifugal concentrator tube (Amicon Ultra-4 Ultracel-10K).

The ATCase activity was assayed by monitoring the production of carbamoyl aspartate from CP and L-aspartate by Ceriotti's colorimetric method (Prescott & Jones, 1969) with minor modifications. Briefly, 0.5 ml of a reaction mixture containing 200 m*M* Tris–HCl pH 7.9, 30 m*M* L-aspartate and purified ATCase was pre-incubated in a 1.5 ml quartz cuvette at 310 K for 5 min and the enzymatic reaction was then started by adding CP to a final concentration of 1.3 m*M*. CP was dissolved in ice-cold distilled water just before measurement. After standing for 15 min at 310 K, the reaction was stopped and 0.5 ml of a 1:1 mixture of 0.5% antipyrine in 50% sulfonic acid and 0.8% diacetylmonoxime in 5% acetic acid was added. Colorimetric development of the diazine produced from the carbamoyl aspartate and diacetylmonoxime was performed at 333 K for 2 h in the dark and the A_{466} was measured. The concentration of the carbamoyl aspartate produced was estimated from the A_{466} values of standard solutions containing carbamoyl aspartate at known concentrations. The typical specific activity of the purified TcATCase was 9 μmol min^{-1} mg^{-1} and the K_m values for CP and L-aspartate were estimated to be 0.03 and 29.4 m*M*, respectively.

TcATCase was purified to apparent homogeneity as shown by SDS–PAGE (Fig. 1), with a yield of about 2 mg from a 1000 ml culture. Gel-filtration chromatography with TSK-gel G3000SWXL (7.8 × 300 mm, Tosoh) and dynamic light-scattering analysis using DynaPro Titan (Wyatt Technology) both indicated that the purified enzyme existed as a homotrimer in solution.

2.2. Crystallization and X-ray data collection

All crystallization experiments were performed by the sitting-drop vapour-diffusion technique in 96-well Corning CrystalEX micro-

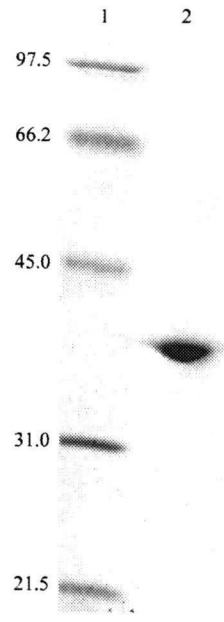

Figure 1
12.5% SDS–PAGE gel stained with Coomassie Brilliant Blue R-250 showing the apparent homogeneity of the purified TcATCase. Lane 1, molecular-weight markers (kDa); lane 2, TcATCase purified using a His-Trap FF column.

Table 1
Statistics of data collection and processing.

Values in parentheses are for the highest resolution shell.

	Ligand-free TcATCase	TcATCase–CP complex
Wavelength (Å)	0.900 (SPring-8 BL44XU)	1.000 (SPring-8 BL41XU)
Space group	$P1$	$P2_1$
Unit-cell parameters (Å, °)	a = 78.42, b = 79.28, c = 92.02, α = 69.56, β = 82.90, γ = 63.25	a = 88.41, b = 158.38, c = 89.00, β = 119.66
Solvent content† (%)	48	51
Frame number	222	180
Resolution range (Å)	50.0–2.8 (2.90–2.80)	50.0–1.60 (1.66–1.60)
No. of reflections	103124	946629
Unique reflections	44850	277190
Mosaicity	0.90	0.21
Redundancy	2.3 (2.3)	3.4 (3.4)
Completeness (%)	97.7 (98.4)	95.3 (91.4)
R_{merge}‡ (%)	7.4 (38.9)	6.5 (39.9)
Mean $I/\sigma(I)$	15.8 (4.4)	11.7 (3.9)

† Assuming the presence of six molecules in the asymmetric unit. ‡ $R_{merge} = \sum_{hkl}\sum_i |I_i(hkl) - \langle I(hkl)\rangle| / \sum_{hkl}\sum_i I_i(hkl)$, where $I_i(hkl)$ is the intensity of the ith observation of reflection hkl.

plates with a conical flat bottom (Hampton Research). In the initial screening for crystallization conditions, a 0.5 µl droplet containing around 10 mg ml^{-1} TcATCase dissolved in 20 mM Tris–HCl pH 7.4 was mixed with an equal volume of reservoir solution and the droplet was allowed to equilibrate against 100 µl reservoir solution at 277 and 293 K. Commercially available screening kits purchased from Hampton Research (Crystal Screen, Crystal Screen 2, Crystal Screen Lite and SaltRx) and Emerald BioStructures (Wizard I, Wizard II, Cryo I and Cryo II) were used as reservoir solutions. Of the 434 conditions screened, condition No. 10 from Crystal Screen Lite [15%(*w*/*v*) PEG 4000, 0.1 *M* sodium acetate pH 4.6, 0.2 *M* ammonium acetate] gave tiny plate-shaped crystals at 277 K. The condition was then optimized using 154 conditions by varying the PEG concentration (4–16%), the buffer pH (3.6–5.6) and the temperature (277 and 293 K) using PEG 3350, which is a monodisperse and high-purity polyethylene glycol obtained from Hampton Research, as a precipitant. For the best condition found, the effects of 72 additives on crystallization were examined using Additive Screen kits (Hampton Research) according to the manufacturer's instruction. Cobalt chloride and glycerol improved the size of the crystals; moreover, the addition of both additives gave thicker crystals. Currently, crystals larger than 0.2 × 0.1 × 0.01 mm can be grown at 277 K from reservoir solution containing 8–10%(*w*/*v*) PEG 3350, 0.1 *M* acetate buffer pH 4.6, 0.2 *M* ammonium acetate, 0.01 *M* cobalt chloride and 3% glycerol. For cocrystallization with CP, a freshly prepared 100 m*M* CP solution was added to the TcATCase solution to give a final concentration of 5 m*M* and crystallization was conducted as described above. Crystals of similar shape and size were obtained.

X-ray diffraction experiments were performed on the BL44XU beamline (λ = 0.900 Å; equipped with a Bruker DIP-6040 detector system) and the BL41XU beamline (λ = 1.000 Å; equipped with a Rayonix CCD MX225HE detector) at SPring-8 (Harima, Japan) and on the BL17A beamline (λ = 1.000 Å; equipped with an ADSC Quantum 270 detector) at Photon Factory (Tsukuba, Japan). A crystal mounted in a nylon loop was transferred and soaked briefly in reservoir solution supplemented with 20%(*w*/*v*) glycerol and then flash-cooled by rapidly submerging it in liquid nitrogen. Diffraction data were collected under cryocooled conditions at 100 K. Images were recorded with an oscillation angle of 1°, an exposure time of 1 s per frame and a crystal-to-detector distance of 150 mm and were processed with the *HKL*-2000 software package (Otwinowski & Minor, 1997).

3. Results and discussion

His_6-tagged TcATCase (38 kDa) could be purified to homogeneity by one-step purification using His-Trap FF column chromatography (Fig. 1). The molecular weight of the purified enzyme estimated by gel-filtration chromatography (134 kDa) and dynamic light scattering (102 kDa; R_h = 4.3 nm, polydispersity = 13.9%, mass = 100%) indicated that the enzyme probably exists as a homotrimer in solution.

Crystals of ligand-free TcATCase were obtained at 277 K from reservoir solution containing 8–10%(*w*/*v*) PEG 3350, 0.1 *M* acetate buffer pH 4.6, 0.2 *M* ammonium acetate, 0.01 *M* cobalt chloride and 3% glycerol and reached maximum dimensions within two weeks (Fig. 2*a*). TcATCase complexed with CP was also crystallized by the cocrystallization method under the same conditions within 2 d (Fig. 2*b*). Analyses of the symmetry and systematic absences in the recorded diffraction patterns indicated that the crystals of ligand-free TcATCase belonged to the triclinic space group $P1$, with unit-cell parameters a = 78.42, b = 79.28, c = 92.02 Å, α = 69.56, β = 82.90, γ = 63.25°, whereas those of TcATCase complexed with CP belonged to the monoclinic space group $P2_1$, with unit-cell parameters a = 88.41, b = 158.38, c = 89.00 Å, β = 119.66°. Assuming the presence of two His_6-tagged TcATCase trimers (6 × 38 kDa) in the asymmetric unit, the V_M values are 2.3 and 2.5 Å^3 Da^{-1} for the triclinic and monoclinic

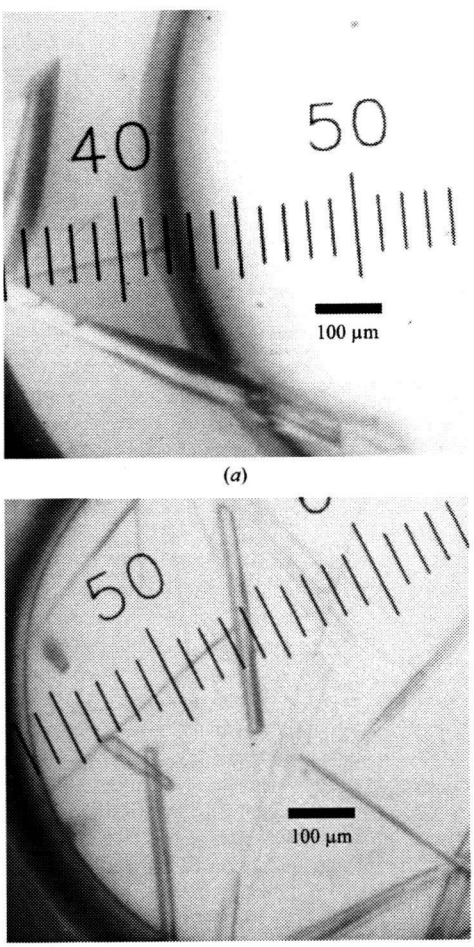

(*a*)

(*b*)

Figure 2
Crystals of (*a*) ligand-free TcATCase and (*b*) TcATCase complexed with carbamoyl phosphate obtained by the sitting-drop vapour-diffusion method using PEG 3350 as a precipitant.

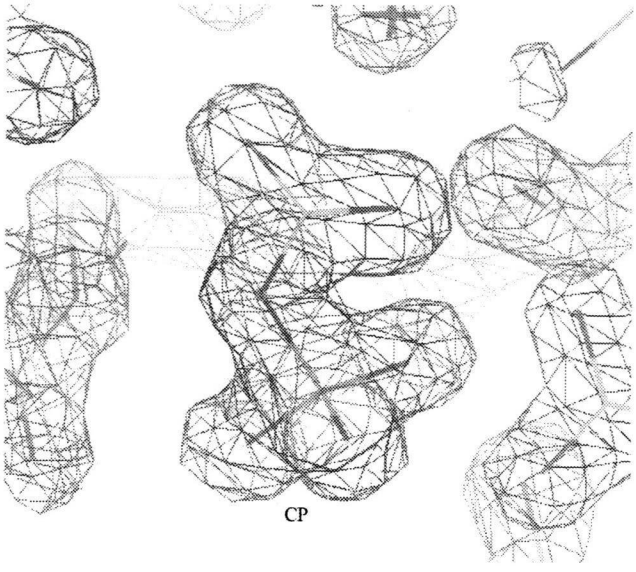

Figure 3
The $2F_o - F_c$ electron-density map around the bound CP in the TcATCase–CP complex structure contoured at 2σ. The structure is currently refined to R = 0.151 (1.6 Å resolution).

crystal forms, respectively; these values are within the range commonly observed for protein crystals (Matthews, 1968). A data set to 2.8 Å resolution (44 850 unique reflections) was obtained for ligand-free TcATCase after merging 103 124 reflections recorded on 222 images, while 277 190 unique reflections to 1.6 Å resolution were produced from 946 629 measured reflections on 180 images for TcATCase complexed with CP. Statistics of data collection and processing are shown in Table 1.

Attempts to solve the structures of both crystal forms by the molecular-replacement method with the *MOLREP* program (Vagin & Teplyakov, 1997) as implemented within the *CCP*4 package (Collaborative Computational Project, Number 4, 1994) were carried out using the homotrimeric structure of the catalytic subunit of *P. abyssi* ATCase (PDB code 1ml4; 40.1% amino-acid sequence identity with TcATCase), which showed a higher identity to TcATCase than to the ATCases from *E. coli* (PDB code 2atc; 36.5% identity), *B. subtilis* (PDB code 2at2; 32.5% identity), *S. acidocaldarius* (PDB code 2be9; 36.8% identity), *Moritella profunda* (PDB code 2be7; 37.7% identity), *Methanococcus jannaschii* (PDB code 2rgw; 38.6% identity) and *A. aeolicus* (PDB code 3d6n; 21.2% identity). A promising solution with two homotrimers per asymmetric unit was obtained for both the ligand-free TcATCase (correlation coefficient and R factor of 0.551 and 49.0%, respectively) and the TcATCase–CP complex (correlation coefficient and R factor of 0.615 and 50.9%, respectively). The models were subsequently subjected to rigid-body refinement and gave R factors of 44.8% and 44.4% for ligand-free TcATCase and the TcATCase–CP complex, respectively. Refinement of the structures is currently in the final stages. Clear electron densities for the entire protein part and the bound CP were observed for the TcATCase–CP complex (Fig. 3), but the loop of the CP-binding site (Cys85–Thr95) was disordered in the ligand-free TcATCase. The suppression of the flexibility of the loop by the bound CP may lead to the different crystal form and the enhanced X-ray diffraction of the crystals of the TcATCase–CP complex. We are now trying to prepare crystals of TcATCase complexed with potential inhibitors found in the Chemical Library of the Chemical Biology Research Initiative, University of Tokyo by *in silico* screening. Since the enzymes of the *de novo* pyrimidine-biosynthetic pathway have great potential as primary targets of chemotherapy (Urbina & Docampo, 2003), the detailed structures of TcATCase complexed with these compounds will help in structure-based drug design aimed at Chagas disease.

We thank all staff members of beamlines BL41XU and BL44XU at SPring-8 and BL17A at Photon Factory for their help with the X-ray diffraction experiments. This work was supported by a grant from the Targeted Proteins Research Program (TPRP) and was supported in part by a grant-in-aid for Creative Scientific Research (18GS0314 to KK) from the Japan Society for the Promotion of Science and a grant-in-aid for Scientific Research on Priority Areas (18073004) from the Japanese Ministry of Education, Science, Culture, Sports and Technology.

References

Aoki, T. (1994). *Jpn. J. Parasitol.* **43**, 1–10.
Aoki, T. & Oya, H. (1987). *Comput. Biochem. Physiol. B*, **87**, 143–150.
Coleman, P. F., Suttle, D. P. & Stark, G. R. (1977). *J. Biol. Chem.* **252**, 6379–6385.
Collaborative Computational Project, Number 4 (1994). *Acta Cryst.* D**50**, 760–763.
De Vos, D., Van Petegem, F., Remaut, H., Legrain, C., Glansdorff, N. & Van Beeumen, J. J. (2004). *J. Mol. Biol.* **339**, 887–900.
De Vos, D., Xu, Y., Hulpiau, P., Vergauwen, B. & Van Beeumen, J. J. (2007). *J. Mol. Biol.* **365**, 379–395.
El-Sayed, N. M. *et al.* (2005). *Science*, **309**, 409–415.
Foltermann, K. F., Wild, J. R., Zink, D. L. & O'Donovan, G. A. (1981). *Curr. Microbiol.* **6**, 43–47.
Freund, J. N. & Jarry, B. P. (1987). *J. Mol. Biol.* **193**, 1–13.
Gao, G., Nara, T., Nakajima-Shimada, J. & Aoki, T. (1999). *J. Mol. Biol.* **285**, 149–161.
Gerhart, J. C. & Pardee, A. B. (1964). *Fed. Proc.* **23**, 727–735.
Gerhart, J. C. & Schachman, H. K. (1965). *Biochemistry*, **4**, 1054–1062.
Gutteridge, W. E. & Gaborak, M. (1979). *Int. J. Biochem.* **10**, 415–422.
Honzatko, R. B., Crawford, J. L., Monaco, H. L., Ladner, J. E., Ewards, B. F., Evans, D. R., Warren, S. G., Wiley, D. C., Ladner, R. C. & Lipscomb, W. N. (1982). *J. Mol. Biol.* **160**, 219–263.
Krause, K. L., Volz, K. W. & Lipscomb, W. N. (1985). *Proc. Natl Acad. Sci. USA*, **82**, 1643–1647.
Liu, X., Guy, H. I. & Evans, D. R. (1994). *J. Biol. Chem.* **269**, 27747–27755.
Matthews, B. W. (1968). *J. Mol. Biol.* **33**, 491–497.
Nara, T., Hirayama-Noguchi, Y., Gao, G., Murai, E., Annoura, T. & Aoki, T. (2003). *Int. J. Parasitol.* **33**, 845–852.
Otwinowski, Z. & Minor, W. (1997). *Methods Enzymol.* **276**, 307–326.
Prescott, L. M. & Jones, M. E. (1969). *Anal. Biochem.* **32**, 408–419.
Shepherdson, M. & Pardee, A. B. (1960). *J. Biol. Chem.* **235**, 3233–3237.
Simmer, J. P., Kelly, R. E., Scully, J. L., Grayson, D. R., Rinker, A. G. Jr, Bergh, S. T. & Evans, D. R. (1989). *Proc. Natl Acad. Sci. USA*, **86**, 4382–4386.
Souciet, J. L., Potier, S., Hubert, J. C. & Lacroute, F. (1987). *Mol. Gen. Genet.* **207**, 314–319.
Stevens, R. C., Reinisch, K. M. & Lipscomb, W. N. (1991). *Proc. Natl Acad. Sci. USA*, **88**, 6087–6091.
Urbina, J. A. (2002). *Curr. Pharm. Des.* **8**, 287–295.
Urbina, J. A. & Docampo, R. (2003). *Trends Parasitol.* **19**, 495–501.
Vagin, A. & Teplyakov, A. (1997). *J. Appl. Cryst.* **30**, 1022–1025.
Van Boxstael, S., Cunin, R., Khan, S. & Maes, D. (2003). *J. Mol. Biol.* **326**, 203–216.
Vitali, J. & Colaneri, M. J. (2008). *Acta Cryst.* F**64**, 776–780.
Wiley, D. C., Evans, D. R., Warren, S. G., McMurray, C. H., Edwards, B. F., Franks, W. A. & Lipscomb, W. N. (1972). *Cold Spring Harb. Symp Quant. Biol.* **36**, 285–290.
Wiley, D. C. & Lipscomb, W. N. (1968). *Nature (London)*, **218**, 1119–1121.
Zhang, P., Martin, P. D., Purcarea, C., Vaishnav, A., Brunzelle, J. S., Fernando, R., Guy-Evans, H. I., Evans, D. R. & Edwards, B. F. (2009). *Biochemistry*, **48**, 766–778.

THE JOURNAL OF BIOLOGICAL CHEMISTRY VOL. 284, NO. 46, pp. 31827–31833, November 13, 2009

Three Redox States of *Trypanosoma brucei* Alternative Oxidase Identified by Infrared Spectroscopy and Electrochemistry[S]

Received for publication, August 26, 2009, and in revised form, September 16, 2009 Published, JBC Papers in Press, September 19, 2009, DOI 10.1074/jbc.M109.059980

Amandine Maréchal[‡1], Yasutoshi Kido[§2], Kiyoshi Kita[§3], Anthony L. Moore[¶4], and Peter R. Rich[‡5]

From the [‡]Glynn Laboratory of Bioenergetics, Institute of Structural and Molecular Biology, University College London, Gower Street, London WC1E 6BT, United Kingdom, the [§]Department of Biomedical Chemistry, Graduate School of Medicine, University of Tokyo, Hongo 7-3-1, Bunkyo-ku, Tokyo 113-0033, Japan, and the [¶]Department of Biochemistry and Biomedical Sciences, School of Life Sciences, University of Sussex, Falmer, Brighton BN1 9QG, United Kingdom

Electrochemistry coupled with Fourier transform infrared (IR) spectroscopy was used to investigate the redox properties of recombinant alternative ubiquinol oxidase from *Trypanosoma brucei*, the organism responsible for African sleeping sickness. Stepwise reduction of the fully oxidized resting state of recombinant alternative ubiquinol oxidase revealed two distinct IR redox difference spectra. The first of these, signal 1, titrates in the reductive direction as an $n = 2$ Nernstian component with an apparent midpoint potential of 80 mV at pH 7.0. However, reoxidation of signal 1 in the same potential range under anaerobic conditions did not occur and only began with potentials in excess of 500 mV. Reoxidation by introduction of oxygen was also unsuccessful. Signal 1 contained clear features that can be assigned to protonation of at least one carboxylate group, further perturbations of carboxylic and histidine residues, bound ubiquinone, and a negative band at 1554 cm^{-1} that might arise from a radical in the fully oxidized protein. A second distinct IR redox difference spectrum, signal 2, appeared more slowly once signal 1 had been reduced. This component could be reoxidized with potentials above 100 mV. In addition, when both signals 1 and 2 were reduced, introduction of oxygen caused rapid oxidation of both components. These data are interpreted in terms of the possible active site structure and mechanism of oxygen reduction to water.

Mitochondria from many higher plants possess, in addition to the conventional cytochrome *c* oxidase, a second terminal oxidase that oxidizes ubiquinol (1–3). In thermogenic plants this alternative oxidase (AOX)[6] plays a key role in the release of heat for pollination purposes or for maintaining a warm environment within the flower at low ambient temperatures. In nonthermogenic plants its function is still under debate; proposed roles include maintaining tricarboxylic acid cycle turnover under high cytosolic phosphorylation potentials, defense against oxidative stress, and growth rate and energy charge homeostasis (4). AOX is also found in species of fungi, green algae, bacteria, and protozoa (5) and, more recently, in mollusks, nematodes, and chordates (6). Of particular importance, however, is its presence in pathogenic protozoa such as the blood parasite *Trypanosoma brucei* (7) and the intestinal parasite *Cryptosporidium parvum* (8, 9). *T. brucei* is a parasite that causes African sleeping sickness in humans and Nagana in livestock and is transmitted by the tsetse fly (7). The bloodstream forms of *T. brucei* appear to depend solely on its alternative oxidase (TAO) for respiration. Because the protein is absent from the mammalian host, TAO is an attractive and important chemotherapeutic target for African trypanosomiasis (7–10). In this respect it is interesting to note that ascofuranone, isolated from the pathogenic fungus *Ascochyta visiae*, specifically and potently inhibits the quinol oxidase activity of TAO (11) and rapidly kills the parasites. In addition, the chemotherapeutic efficacy of ascofuranone *in vivo* has been confirmed (12).

Compared with other respiratory chain complexes, the structure and mechanism of AOX are poorly characterized because of difficulties encountered in purification and a dearth of spectroscopic signatures. It has been proposed from sequence comparisons that AOX is a nonheme diiron carboxylate protein in which the metal atoms are ligated by glutamic acid and histidine residues within a four-helix bundle (1, 2, 13). The requirement for such a tertiary structural motif, as well as the necessary spacing between the iron-ligating amino acids, imposes considerable constraints upon overall possible three-dimensional structure and, consequently, its attachment to the membrane. The current model of the AOX, supported by mutagenesis studies, predicts a monotopic integral membrane protein (2, 13–15) associating with one leaflet of the lipid

[S] The on-line version of this article (available at http://www.jbc.org) contains supplemental Figs. S1–S3 and Table S1.

[1] Supported by a Wellcome Trust ViP award.
[2] Supported in part by Grant-in-aid for Young Scientists (B) 21790402.
[3] Supported by Creative Scientific Research Grant 18GS0314, Grant-in-aid for Scientific Research on Priority Areas 18073004 from the Japanese Society for the Promotion of Science, and a Targeted Proteins Research Program from the Japanese Ministry of Education, Science, Culture, Sports and Technology.
[4] Supported by the Biotechnology and Biological Sciences Research Council and the Prime Minister's Initiative 2 (Connect) fund for collaborative twinning with KK.
[5] Supported by Biotechnology and Biological Sciences Research Council Research Grant BB/H000097/1. To whom correspondence should be addressed. Tel.: 44-20-7679-7746; Fax: 44-20-7679-7096; E-mail: prr@ucl.ac.uk.

[6] The abbreviations used are: AOX, alternative oxidase; ATR, attenuated total reflection; δ_{IP}, in plane bending; FTIR, Fourier transform infrared; TAO, trypanosomal alternative oxidase; rTAO, recombinant TAO expressed in a heme-deficient strain of *E. coli*; ν_s and ν_{as}, symmetric and asymmetric stretching, respectively.

bilayer. Although analyses of yeast and trypanosomal enzymes have established that iron is required for activity (16, 17), early investigations of either mitochondria or partially purified protein failed to reveal spectroscopic signatures of its active site (18, 19). The first spectroscopic evidence for iron involvement was provided by Berthold *et al.* (20), who reported two EPR signals in *Escherichia coli* membranes that contained an overexpressed, truncated but active *Arabidopsis thaliana* alternative oxidase (AOX1a) fused to a maltose-binding protein. A signal around $g = 15$, observed with parallel mode EPR in reduced samples, was attributed to the diferrous state. A second signal, observed only after reaction of this state with oxygen, was assigned to a mixed valence ($Fe^{II}Fe^{III}$) form. More recently, Affourtit and Moore (21) prepared an active AOX protein from *Arum maculatum*. Parallel mode EPR studies (22) confirmed the presence of the diferrous signal in the reduced protein but attempts to generate the mixed valence signal of Berthold *et al.* (20) were not successful. Further spectroscopic tools are clearly desirable to resolve these inconsistencies, and, with this aim in mind, we report here the first electrochemical/FTIR study of a highly purified and stable preparation of recombinant AOX (rTAO) from *T. brucei*.

EXPERIMENTAL PROCEDURES

Isolation of rTAO—TAO was expressed in *E. coli* FN102 (Δ*hemA*) as described previously (23). In brief, rTAO was extracted by 1.4% (w/v) *n*-octyl-β-D-glucopyranoside, and, because rTAO was fused with an N-terminal histidine tag, solubilized rTAO was purified by cobalt affinity chromatography. The solubilized enzyme was bound to the cobalt affinity resin in the presence of detergent, and 100% of the rTAO activity was recovered from the column when *n*-octyl-β-D-glucopyranoside in the washing and elution buffers was exchanged with 0.042% (w/v) *n*-dodecyl-β-D-maltopyranoside. Finally, purified rTAO was obtained by two-step elution with 165 mM and 200 mM imidazole, which resulted in a very efficient purification of active rTAO in the presence of *n*-dodecyl-β-D-maltopyranoside (see supplemental Fig. S1). Specific activity of the final preparation was 207 μmol/min per mg using 150 μM ubiquinol-1.

ATR-FTIR Spectroscopy—Mid-IR spectra were recorded in ATR mode with a Bruker IFS/66S FTIR spectrophotometer fitted with a liquid nitrogen-cooled MCT-A detector at 4 cm^{-1} resolution, giving an accuracy of cited frequencies of ±1 cm^{-1}.

Sample Preparation—To remove the imidazole and to favor the interaction of the protein with the ATR prism surface, 100 μg of rTAO was diluted in 2.5 ml of 1 mM potassium phosphate buffer, pH/pD 7.0, and centrifuged at 450,000 × *g*, 4 °C, for 30 min. The pellet was resuspended with 2.5 ml of the same buffer and centrifuged for 15 min under the same conditions. The pellet was finally resuspended with 8 μl of 1 mM potassium phosphate, pH/pD 7.0. This solution was then quickly put on the ATR prism and dried under a nitrogen flow (4–5 min). The dried protein was rewetted with 10 μl of a 1 mM potassium phosphate buffer, pH/pD 7.0. The protein sample was stable with an amide II band intensity of 0.1–0.2.

Electrochemically Induced Spectroscopy—An ATR-FTIR-compatible cell with a platinum mesh working electrode was built on top of the sample layer. It was connected via a Vycor frit to a platinum sheet counter and Ag/AgCl reference electrodes (24). The chamber was filled with a freshly prepared mediator solution, and the sample was allowed to equilibrate for 1 h before starting any redox experiment. Buffer alone was placed in the reference/counter electrode chamber. All of the potential values are quoted relative to the normal hydrogen electrode.

Reduced minus oxidized spectra were induced electrochemically in 100 mM potassium phosphate, 100 mM KCl at pH/pD 7.0 and containing 500 μM potassium ferricyanide and 100 μM benzyl viologen as redox mediators. Working electrode potentials were +550 mV for oxidation and −400 mV for reduction. IR difference spectra were measured by recording a background spectrum (500 interferograms) at one potential, then switching to the second potential and recording a sample spectrum after a 13-min equilibration. Redox cycles were repeated 40 times in H_2O buffer (30 times in D_2O buffer), and reductive and oxidative spectra were averaged to produce the redox spectra shown.

For redox titration experiments, two different mixtures of mediators in 100 mM potassium phosphate, 100 mM KCl at pH 7.0 were tested: (i) 200 μM indigo trisulfonate ($n = 2$; $E_0' = -81$ mV) + 200 μM ruthenium hexamine ($n = 1$; $E_0' = +20$ mV) + 200 μM 2,4-naphthoquinone disulfonic acid ($n = 2$; $E_0' = +120$ mV) or (ii) 200 μM indigo trisulfonate + 200 μM 2,4-naphthoquinone disulfonic acid + 200 μM phenazine methosulfate ($n = 2$; $E_0' = +80$ mV) + 100 μM gallocyanine ($n = 2$; $E_0' = +20$ mV) + 1 mM ferricyanide ($n = 1$; $E_0' = +430$ mV). IR difference spectra were measured against a background spectrum of the fully oxidized (air-oxidized) sample. Reductive potentials between +200 mV and −100 mV were applied, and 15–20 min were required between two potential steps to achieve stability of the intensity of the two peak/troughs at 1658/1641 and 1544/1554 cm^{-1}. The signal amplitudes were expressed as a fraction of those of a reduced minus air-oxidized spectrum. They were plotted against potentials and simulated with the Nernstian equation,

$$y = \frac{1}{1 + \exp\left(\frac{(E_{1/2} - x) \times nF}{RT}\right)} \quad \text{(Eq. 1)}$$

where y is the oxidized fraction of TAO, x is the potential of the solution (in V), $E_{1/2}$ is the midpoint potential for the redox couple at pH 7.0, and n is the number of electrons involved in the reaction ($F = 96\,485$ C·mol^{-1}; $r = 8.314$ J·mol^{-1}·K^{-1}; $T = 298$ K). The reproducible data in Fig. 2 were obtained from a single 4-h titration.

Calculations of Vibrational Spectra—IR-active normal modes of tyrosine (Tyr-OH), tyrosinate (Tyr-O^-), and tyrosyl (Tyr-$O^•$) were calculated on the UCL Legion parallel supercomputer cluster using Gaussian03 (25) with the B3LYP/6–13G(d) density functional and dataset. Data were obtained both for the zwitterionic free tyrosine as well as for tyrosine in a modified tripeptide (NH_2-Gly-Tyr-Gly-$COCH_3$) to better reflect protein environment. Molecular structures were first built with Facio (2006). Structures were then energy-minimized before calcu-

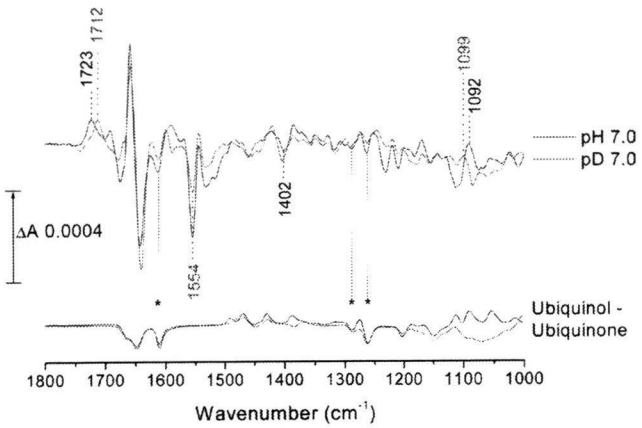

FIGURE 1. **Reduced minus oxidized IR difference spectrum of rTAO.** Reduction oxidation transformations were induced electrochemically in 100 mM potassium phosphate, 100 mM KCl at pH (*black trace*)/pD (*red trace*) 7.0 and containing 500 μM potassium ferricyanide and 100 μM benzyl viologen as redox mediators. Working electrode potentials were −400 mV for reduction and +550 mV for oxidation. For further details, see "Experimental Procedures." Published ubiquinol-10 minus ubiquinone-10 redox spectra recorded in both H_2O (*black*) and D_2O (*red*) media are also displayed for qualitative comparisons (37).

lating frequencies. Frequencies cited have been multiplied by the published scaling factor of 0.9614 (25).

RESULTS AND DISCUSSION

Secondary Structure Estimation—Information on protein secondary structure can be obtained from analyses of component bands within the amide I envelope of absolute IR absorption spectra (26, 27). Such an analysis performed on the IR spectra of rTAO in both H_2O and D_2O media predicts a minimum of 30% α-helix content in the rTAO secondary structure and up to 64% if rTAO can adopt a coiled-coil arrangement (see supplemental Table S1) (28, 29), as would occur if rTAO is folded to form the predicted four-helix bundle.

Reduced Minus Oxidized FTIR Difference Spectra—IR redox difference spectra of TAO obtained by electrochemistry at pH/pD 7.0 are shown in Fig. 1. The data were recorded in both H_2O (black) and D_2O (red) media to aid assignments. As with most redox proteins, the largest IR bands are found in the amide I (peak/trough at 1658/1641 cm^{-1}) and amide II (peak/trough at 1544/1554 cm^{-1}) regions and most commonly arise from changes in the amide I (predominantly C=O) and amide II (predominantly N–H) bands of the polypeptide backbone amide linkages. The assignment of the 1658/1641 cm^{-1} bands to redox-dependent amide I changes is strengthened by their very weak sensitivity to H/D exchange. In contrast, amide II bands are strongly shifted (≈−100 cm^{-1}) by H/D exchange, which is not the case for the 1554/1544 cm^{-1} bands. An estimation of the extent of H/D exchange from absolute IR absorption spectrum of rTAO recorded in D_2O *versus* H_2O (30) indicated that it was more than 95%. Hence, it is unlikely that the lack of shift was caused by poor H/D exchange, and other possible origins of the trough/peak at 1554/1544 cm^{-1} are discussed below.

An informative feature in the redox spectra is the positive peak at 1723 cm^{-1} in H_2O that is downshifted to 1712 cm^{-1} on H/D exchange. Bands in this frequency range with such H/D shifts are generally characteristic of protonated carboxyl groups (31, 32). There is no associated trough of equal magnitude in this region, ruling out the possibility that the carboxyl group(s) is also protonated in the oxidized state. However, a trough of roughly equal intensity was observed at 1402 cm^{-1}, slightly up-shifted (+2 cm^{-1}) on H/D exchange, together with a broad trough that underlies sharper bands in the 1560–1500 cm^{-1} amide II region. Taken together, these bands suggest the loss on reduction of the ν_s and ν_{as} vibrational modes of a deprotonated carboxylate group at 1402 and ~1530 cm^{-1} that is linked with the appearance of the 1723 cm^{-1} C=O peak of its protonated form. Hence, we conclude that reduction of rTAO results in the net protonation of one or more carboxylate groups. Deconvolution of both the H_2O and D_2O spectra with multiple Gaussian functions in the 1750-1700 cm^{-1} region (see supplemental Fig. S2) suggests that more than one carboxyl group may contribute. The best fit was obtained with two carboxyl groups being protonated (peaks at 1725 and 1717 cm^{-1} in H_2O, 1715 and 1709 cm^{-1} in D_2O) and one protonated carboxyl group changing conformation/environment on reduction (trough/peak at 1749/1735 cm^{-1} in H_2O, shifted by −8 cm^{-1} and more evident in the D_2O spectrum).

Other features around 1100 cm^{-1} are likely to arise from histidine changes (31, 33). In particular, the intense peak at 1092 cm^{-1}, upshifted to 1099 cm^{-1} in D_2O, is consistent with perturbation of an Nτ-protonated histidine bound by its Nπ to a metal center (34), as is found in the active sites of other homologous diiron proteins (35).

Finally, because reduced ubiquinone-9 is known to be the TAO electron donor in the bloodstream form of the trypanosome (36), we compared the rTAO redox spectra with published ubiquinone redox spectra recorded in both H_2O and D_2O media (37). Several bands are evident that correspond to those seen in the reference ubiquinone spectra (Fig. 1), particularly the bands at 1263 and 1289 cm^{-1} (arising from methoxy/quinone ring modes) and at 1612 cm^{-1} (from quinone C=C bonds) (38).

Redox Titration—The presence of an FTIR redox signature in rTAO provided a means to determine the redox properties of its active site by controlled potentiometry in a combined electrochemical/ATR-FTIR device (24). Redox mediators were chosen to cover the potential range from +200 to −100 mV (see "Experimental Procedures"). Fig. 2*A* presents the spectra recorded during the first reductive titration of a freshly prepared protein layer in 100 mM potassium phosphate, 100 mM KCl, at pH 7.0. The extent of reduction was estimated from the magnitudes of the two peak/troughs at 1658/1641 and 1544/1554 cm^{-1} and, typically, 15–20 min were required between two potential steps to allow their stabilization. The extent of reduction is plotted against ambient potential in Fig. 2*B*. It displayed the Nernstian behavior expected for an $n = 2$ reduction with a midpoint potential of +80 mV at pH 7.0 (see overlays in Fig. 2*B*). However, attempts to reverse the titration without hysteresis in the oxidative direction were unsuccessful, and no reoxidation was observable until potentials above +500 mV were applied (see below). Hence, it is not possible to conclude that the behavior seen in the reductive direction represents the equilibrium thermodynamic properties of this redox transition.

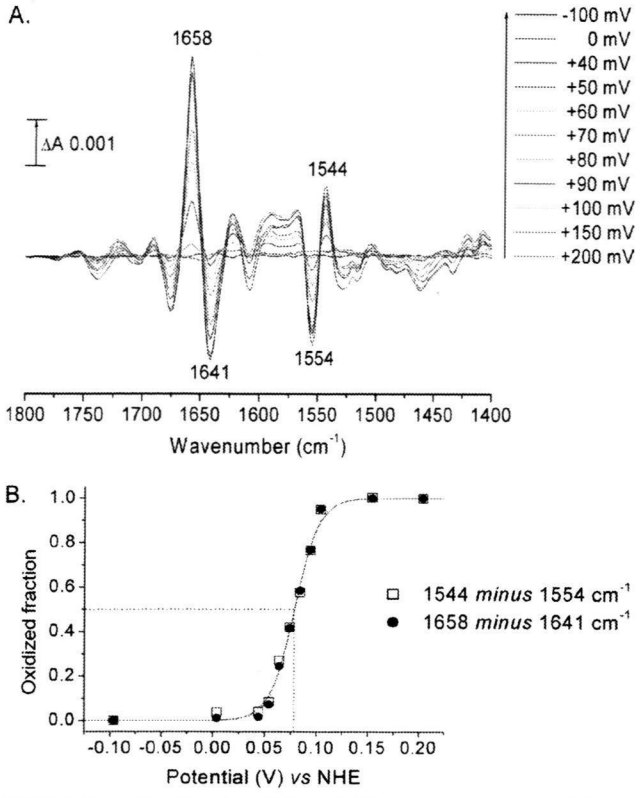

FIGURE 2. **Reductive titration of rTAO.** *A*, difference spectra recorded during a reductive titration in 100 mM potassium phosphate, 100 mM KCl at pH 7.0 (see "Experimental Procedures"). *B*, plots of peak/trough intensities at 1658/1641 and 1544/1554 cm^{-1} *versus* potential. Data were simulated with a Nernst-derived equation for an $n = 2$ component with $E_{1/2} = 79$ mV.

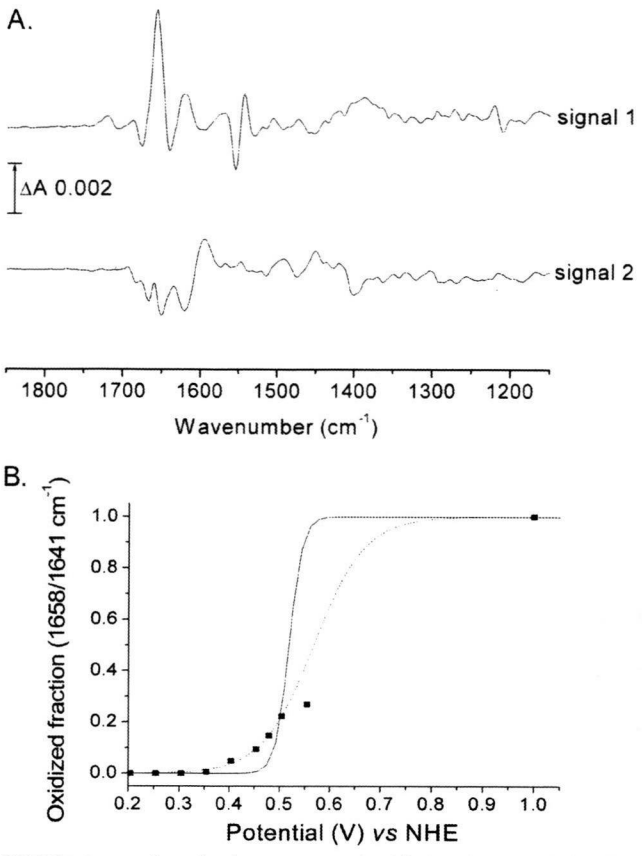

FIGURE 3. **Separation of redox spectra and oxidative titration of signal 1.** *A*, a fully oxidized spectrum was recorded and use as a background. Potential was set to −10 mV, and signal 1 was recorded after 20 min. A new background spectrum was then recorded, and signal 2 was observed to develop at 1 h. *B*, oxidative titration of signal 1 at pH 7.0 with a mixture of redox mediators containing ferricyanide. Data were simulated with a Nernst-derived equation (see "Experimental Procedures") for an $n = 2$ component with $E_{1/2} = 520$ mV (*solid line*) or for an unrestricted fit which gave $n = 0.6$ and $E_{1/2} = 510 \pm 30$ mV (*dotted line*). The maximum intensity of signal 1 was determined by the addition of dioxygen to the fully reduced state.

Introduction of oxygen into the sample when this component had become reduced also failed to promote reoxidation, indicating that this reduced state is not the oxygen-reactive species.

Further investigations revealed that there was a second redox component that was becoming reduced much more slowly than the redox component represented by the two peak/troughs at 1658/1641 and 1544/1554 cm^{-1} and termed "signal 1." This could be detected most clearly after reduction of a fully oxidized sample for 20 min at −10 mV, at which time signal 1 was fully developed and the second component remained mostly oxidized (Fig. 3*A*, *signal 1*). Maintenance of the ambient potential at −10 mV led to the appearance of a second distinct redox IR spectrum that we have termed "signal 2." Its reduction was slow (1 h at −10 mV) but, in contrast to signal 1, could be reoxidized slowly by moderate oxidizing potentials (1 h at +200 mV). A full titration of this second redox couple could not be achieved because of overlap with signal 1 and its very slow rate of redox equilibration. Nevertheless, by prereduction of both signals 1 and 2, followed by reoxidation of signal 2, a reduced minus oxidized spectrum of signal 2 alone could be obtained (Fig. 3*A*, *signal 2*), and an approximate midpoint potential around +50 mV could be estimated. Signals 1 and 2 are quite distinct components. For example, there is no signature of protonated carboxyl group at 1723 cm^{-1} or evidence of bands at 1544/1554 cm^{-1} in signal 2. These spectra are not shown below 1200 cm^{-1} because the redox mediators used also absorb in this region, and no corrections for their contributions were made.

After full reduction of both signals 1 and 2, the fully oxidized starting state of rTAO could be regenerated within the time scale of recording by introduction of O_2 into the electrochemistry cell. This contrasts markedly with the oxygen-insensitive behavior observed when only signal 1 was reduced. After reoxidation with molecular oxygen when signals 1 and 2 were reduced, signals 1 and 2 could then be titrated as before. These observations show that both redox components must be reduced to produce a form that can react with oxygen to regenerate the fully oxidized state.

In an attempt to titrate signal 1 oxidatively, redox titrations were performed with a mixture of mediators containing ferricyanide to allow equilibration at higher potentials (see "Experimental Procedures"). After full reduction of signals 1 and 2 (approximately 1.5 h at −10 mV) and oxidation of signal 2 only (approximately 1 h at +200 mV), potentials were stepped to higher values (see Fig. 3*B*). After 2.5 h with potentials as high as +550 mV, only a fraction (≈25%) of signal 1 was oxidized. We verified this was not due to protein instability by reduction back to the fully reduced form of rTAO and reintroduction of O_2, thereby regenerating 100% of the fully oxidized state. These

observations suggest that potentials in excess of +550 mV are required for full signal 1 reoxidation, which is beyond the limit of accessible electrochemistry with the platinum grid/ferricyanide system. This behavior explains the low signal amplitudes of the rTAO data of Fig. 1 because the data are an average of cyclical reductions and oxidations without introduction of oxygen to regenerate the oxidized state fully and without a very long time at reducing potentials to reduce signal 2 fully. The cycle of reduction of signal 1 and signal 2 followed by injection of O_2 into the electrochemistry cell to restore the fully oxidized resting state could be repeated reproducibly over many cycles, indicating that the enzyme itself remained very stable during the course of these investigations.

By comparison of band intensities at 1263 and 1612 cm^{-1} of a full redox spectrum of an optimized protein layer with those of a standardized solution of ubiquinone-10 in chloroform (see supplemental Fig. S3), a ubiquinone concentration in the layer was estimated to be approximately 4 mM. Previously, it has been shown that a layer of bovine cytochrome *c* oxidase (molecular mass, 204,000 Da; amide II band, approximately 0.25 ΔA) is maximally 1.8 mM (based on perfect packing) (39). Hence, the rTAO concentration (molecular mass, 34,000 Da; amide II band, 0.22 ΔA) could be up to 9 mM. As a result, it is concluded that the rTAO has retained ubiquinone such that its Q site is partially occupied with substrate ubiquinone.

Relevance to Catalytic Cycle—This study has revealed two redox processes that have distinct IR signatures, signal 1 and signal 2. Signal 1 could be titrated in the reductive direction where it behaved as if it were an $n = 2$ process with a midpoint potential of +80 mV at pH 7.0. However, the reaction was not reversible over the same potential range, indicating that this does not represent its equilibrium thermodynamic properties, a conclusion confirmed by the observation that even partial reoxidation of signal 1 could be achieved only with potentials of +550 mV. Such behavior can be observed in $n = 2$ redox systems when the one-electron intermediate is highly unstable, such as is seen, for example, in cyclic voltammetric behavior of quinones (40). In this case, reduction is controlled by the low potential reduction of quinone to semiquinone, whereas quinol oxidation is controlled by the high potential step of quinol oxidation to semiquinone. Hence, both oxidative and reductive waves appear only at overpotentials compared with the equilibrium $n = 2$ potential. It is possible that the behavior of signal 1 arises from a similar phenomenon in which it is an $n = 2$ reaction, but with a highly unstable one-electron form. In this case, the true thermodynamic $n = 2$ midpoint potential will lie somewhere between the observable reductive and oxidative waves. It is also possible that reduction of signal 1 by mediators is indirect, being mediated by the ubiquinone that is bound to the protein and that it is the known redox hysteresis of the ubiquinone that gives rise to the signal 1 behavior. A further possibility is that reduction of signal 1 induces a conformational change of the protein, raising the signal 1 potential to much higher values, a type of behavior that has been proposed to explain hysteresis of cytochrome cd_1 redox titrations (41).

Signal 2 behaves more conventionally in that it appears to be reversibly oxidized and reduced over the same potential range, with a midpoint potential around +50 mV. However, its equilibration was far too slow to be able to perform an accurate redox titration to determine whether it had an *n* value of 1 or 2. These slow kinetics are not limited by diffusion of mediators between electrode and protein layer. They most likely arise because of slow equilibration between mediators and the redox group(s) involved.

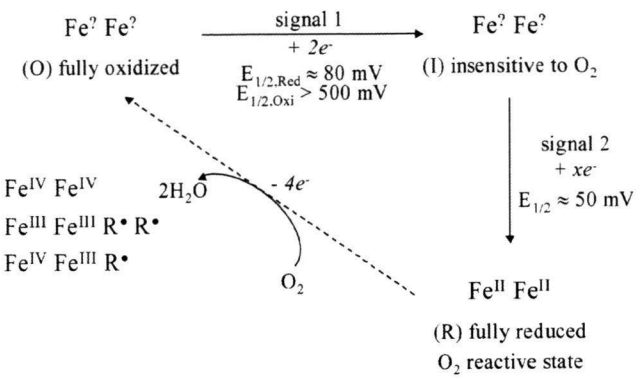

FIGURE 4. **Summary of experimental observations and their relation to the catalytic cycle of reduction of oxygen to water.**

In Fig. 4, a working model is proposed of the relationship between these IR-observed species and the physiological reaction cycle of the 4-electron reduction of dioxygen to water. Starting from the fully oxidized resting state of TAO (O), a 2-electron reduction occurs, represented by signal 1. This produces a species (I) that is insensitive to the presence of dioxygen. The (I) minus (O) IR difference spectrum shows clearly the net protonation of at least one carboxylate residue, and this is likely to give the transition a pH-dependent midpoint potential. In addition, the complexity of the carboxylic acid region changes, indicative of an additional underlying carboxylic acid shift, together with perturbations in the 1100 cm^{-1} region that indicate histidine alterations, are consistent with the proposed involvement of glutamic and histidine residues in the active site (1, 2, 13).

Species (I) can be further reduced, most probably with two electrons, to give a third redox state (R) that is the oxygen-reactive form. (R) must presumably correspond to the diferrous state that gives rise to the spin-coupled $Fe^{II}Fe^{II}$ EPR signal at $g \geq 15$ that was observed in dithionite-reduced samples by Berthold *et al.* (20) and Moore *et al.* (22). The need to reduce TAO fully to react with oxygen to form the (O) state might be related to the observation of Berthold *et al.* that an $Fe^{II}Fe^{III}$ mixed-valence state could only be observed by oxidation of the fully reduced state with oxygen (42). However, because of the differences in protocol details, it is not possible at present to determine whether the mixed-valence form should correspond to (O) or (I).

(R) can react rapidly with dioxygen to regenerate the fully oxidized (O) state. Because 4 electrons are required for reduction of dioxygen to water, the oxidation state of (O) will depend on whether the electrons are provided solely by the two metals, by protein residue(s) that produce radicals, or by substrate ubiquinol. Hence, if the (O) state does indeed result in formation of water, it must be (i) a diferryl center ($Fe^{IV}Fe^{IV}$); (ii) a diferric center plus two radicals ($Fe^{III}Fe^{III}R^{\bullet}R^{\bullet}$); (iii) a mixed-

valence ferryl/ferric center plus a radical ($Fe^{IV}Fe^{III}R^{\bullet}$) (3). All of these species are potentially EPR-silent. Such radicals could arise from amino acids or, possibly, substrate ubiquinol. Reduction of (O) to (I) most likely involves addition of two reducing equivalents into the (O) state that reduce the metals and/or radicals. Finally, it also remains possible that oxygen is incompletely reduced in the (O) state, which could, for example, contain a bound peroxide that becomes reduced in the (O) to (I) transition. Such a species could well explain the irreversibility of the reduction. However, it is difficult to reconcile a peroxide species with the formation of a mixed-valence form, and so this possibility presently seems unlikely.

In the R2 subunit of the ribonucleotide reductase, a well characterized diiron carboxylate protein, a tyrosyl residue is involved in catalysis. The fact that this residue is buried deeply into the protein structure provides it with a peculiar stability (up to several days) (43). Mutagenesis studies of both the plant AOX (44) and TAO (15) have revealed that tyrosine 275 is crucial for catalysis. This tyrosine or, possibly, a nearby tryptophan 206 (*Sauromatum guttatum* numbering) might provide a radical site (44, 45); hence a role for radical(s) in the TAO catalytic cycle seems likely. The sharp H/D-insensitive negative band at 1554 cm^{-1} could arise from the loss of a radical in the (O) to (I) transformation. Radicals of ubiquinone are expected to have a sharp band around 1490 cm^{-1}. IR and Raman features of neutral phenoxyl radical models and tyrosine radicals in proteins show two prominent modes of the neutral phenolic radical identified as ν_{8a}(C–C) at 1550–1610 cm^{-1} and ν_{7a}(C–O) at 1480–1530 cm^{-1}, and the radical state of TyrD in photosystem II shows two bands at 1551 and 1503 cm^{-1} (46–48). Moreover, density functional theory simulations (see "Experimental Procedures") of a neutral tyrosyl radical in both free zwitterionic tyrosine and in a model peptide also predict a strong band at 1554 cm^{-1}. In contrast, the rather limited IR data on tryptophanyl radicals indicate that they have IR bands at higher frequencies (49). Hence, if the 1554 cm^{-1} band does indeed arise from a radical, a tyrosyl species in the (O) state is currently most favored. Ground-state tyrosine in its protonated form is known to have bands at 1508 cm^{-1} and, in the tyrosinate form, at 1547 cm^{-1}. These bands also appear in density functional theory simulations, with an assignment to a normal mode arising from ν(C–O) + ν_s(C–C_{ring}) + δ_{IP}(H–C_{ring}). Hence, if the 1544/1554 cm^{-1} peak/trough in signal 1 does arise from tyrosine, then it most closely resembles the loss of a neutral tyrosyl radical in (O) and formation of a tyrosinate in (I) and (R). In any case, such a stable tyrosyl radical would have to be in an unusual environment in TAO, and stabilization of the tyrosinate state in (I) should make the formation of a radical energetically more facile. Further IR work on TAO and related diiron proteins, in particular a combination of FTIR and EPR analyses of the same redox states, should resolve both the nature of the mixed valence form and the involvement and types of any radicals.

REFERENCES

1. Finnegan, P. M., Soole, K. L., and Umbach, A. L. (2004) *Plant Mitochondria: From Genome To Function*, p. 163, Kluwer Academic Publishers, Dordrecht, The Netherlands
2. Berthold, D. A., and Stenmark, P. (2003) *Annu. Rev. Plant. Biol.* **54,** 497–517
3. Affourtit, C., Albury, M. S., Crichton, P. G., and Moore, A. L. (2002) *FEBS Lett.* **510,** 121–126
4. Moore, A. L., Albury, M. S., Crichton, P. G., and Affourtit, C. (2002) *Trends Plant Sci.* **7,** 478–481
5. McDonald, A. E., and Vanlerberghe, G. C. (2006) *Comp. Biochem. Physiol. D* **1,** 357–364
6. McDonald, A., and Vanlerberghe, G. (2004) *IUBMB Life* **56,** 333–341
7. Chaudhuri, M., Ott, R. D., and Hill, G. C. (2006) *Trends Parasitol.* **22,** 484–491
8. Roberts, C. W., Roberts, F., Henriquez, F. L., Akiyoshi, D., Samuel, B. U., Richards, T. A., Milhous, W., Kyle, D., McIntosh, L., Hill, G. C., Chaudhuri, M., Tzipori, S., and McLeod, R. (2004) *Int. J. Parasitol.* **34,** 297–308
9. Suzuki, T., Hashimoto, T., Yabu, Y., Kido, Y., Sakamoto, K., Nihei, C., Hato, M., Suzuki, S., Amano, Y., Nagai, K., Hosokawa, T., Minagawa, N., Ohta, N., and Kita, K. (2004) *Biochem. Biophys. Res. Commun.* **313,** 1044–1052
10. Nihei, C., Fukai, Y., and Kita, K. (2002) *Biochim. Biophys. Acta* **1587,** 234–239
11. Minagawa, N., Yabu, Y., Kita, K., Nagai, K., Ohta, N., Meguro, K., Sakajo, S., and Yoshimoto, A. (1997) *Mol. Biochem. Parasitol.* **84,** 271–280
12. Yabu, Y., Yoshida, A., Suzuki, T., Nihei, C., Kawai, K., Minagawa, N., Hosokawa, T., Nagai, K., Kita, K., and Ohta, N. (2003) *Parasitol. Int.* **52,** 155–164
13. Andersson, M. E., and Nordlund, P. (1999) *FEBS Lett.* **449,** 17–22
14. Berthold, D. A., Andersson, M. E., and Nordlund, P. (2000) *Biochim. Biophys. Acta* **1460,** 241–254
15. Nakamura, K., Sakamoto, K., Kido, Y., Fujimoto, Y., Suzuki, T., Suzuki, M., Yabu, Y., Ohta, N., Tsuda, A., Onuma, M., and Kita, K. (2005) *Biochem. Biophys. Res. Commun.* **334,** 593–600
16. Minagawa, N., Sakajo, S., Komiyama, T., and Yoshimoto, A. (1990) *FEBS Lett.* **267,** 114–116
17. Ajayi, W. U., Chaudhuri, M., and Hill, G. C. (2002) *J. Biol. Chem.* **277,** 8187–8193
18. Rich, P. R. (1978) *FEBS Lett.* **96,** 252–256
19. Berthold, D. A., and Siedow, J. N. (1993) *Plant Physiol.* **101,** 113–119
20. Berthold, D. A., Voevodskaya, N., Stenmark, P., Gräslund, A., and Nordlund, P. (2002) *J. Biol. Chem.* **277,** 43608–43614
21. Affourtit, C., and Moore, A. L. (2004) *Biochim. Biophys. Acta* **1608,** 181–189
22. Moore, A. L., Carré, J. E., Affourtit, C., Albury, M. S., Crichton, P. G., Kita, K., and Heathcote, P. (2008) *Biochim. Biophys. Acta* **1777,** 327–330
23. Nihei, C., Fukai, Y., Kawai, K., Osanai, A., Yabu, Y., Suzuki, T., Ohta, N., Minagawa, N., Nagai, K., and Kita, K. (2003) *FEBS Lett.* **538,** 35–40
24. Rich, P. R., and Iwaki, M. (2007) *Mol. BioSys.* **3,** 398–407
25. Frisch, M. J., Trucks, G. W., Schlegel, H. B., Scuseria, G. E., Robb, M. A., Cheeseman, J. R., Montgomery, J. A., Jr., Vreven, T., Kudin, K. N., Burant, J. C., Millam, J. M., Iyengar, I. I., Tomasi, J., Barone, V., Mennucci, B., Cossi, M., Scalmani, G., Rega, N., Petersson, G. A., Nakasuji, H., Hada, M., Ehara, M., Toyota, K., Fukuda, R., Hasegawa, J., Ishida, M., Nakajima, T., Honda, Y., Kitao, O., Nakai, H., Klene, M., Li, X., Knox, J. E., Hratchian, H. P., Cross, J. B., Bakken, V., Adamo, C., Jaramillo, J., Gomperts, R., Stratmann, R. E., Yazyev, O., Austin, A. J., Cammi, R., Pomelli, C., Ochterski, J. W., Ayala, P. Y., Morokuma, K., Voth, G. A., Salvador, P., Dannenberg, J. J., Zakrzewski, G., Dapprich, S., Daniels, A. D., Strain, M. C., Farkas, O., Malick, D. K., Rabuck, A. D., Raghavachari, K., Foresman, J. B., Ortiz, J. V., Cui, Q., Baboul, A. G., Clifford, S., Cioslowski, J., Stefanov, B. B., Liu, G., Liashenko, A., Piskorz, P., Komaromi, I., Martin, R. L., Fox, D. J., Keith, T., Al-Laham, M. A., Peng, C. Y., Nanayakkara, A., Challacombe, M., Gill, P. M. W., Johnson, B., Chen, W., Wong, M. W., Gonzalez, C., and Pople, J. A. (2005) *Gaussian 03*, Gaussian, Inc., Wallingford, CT
26. Arrondo, J. L. R., Muga, A., Castresana, J., and Goñi, F. M. (1993) *Prog. Biophys. Mol. Biol.* **59,** 23–56
27. Arrondo, J. L. R., and Goñi, F. M. (1999) *Prog. Biophys. Mol. Biol.* **72,** 367–405
28. Heimburg, T., Schuenemann, J., Weber, K., and Geisler, N. (1996) *Biochemistry* **35,** 1375–1382
29. Reisdorf, W. C., Jr., and Krimm, S. (1996) *Biochemistry* **35,** 1383–1386

30. Glasoe, P. K., and Long, F. A. (1960) *J. Phys. Chem.* **64,** 188–190
31. Barth, A. (2000) *Prog. Biophys Mol. Biol.* **74,** 141–173
32. Rich, P. R., and Iwaki, M. (2005) *Biophysical and Structural Aspects of Bioenergetics*, p. 314, The Royal Society of Chemistry, Cambridge, UK
33. Iwaki, M., Yakovlev, G., Hirst, J., Osyczka, A., Dutton, P. L., Marshall, D., and Rich, P. R. (2005) *Biochemistry* **44,** 4230–4237
34. Noguchi, T., Inoue, Y., and Tang, X.-S. (1999) *Biochemistry* **38,** 10187–10195
35. Solomon, E. I., Brunold, T. C., Davis, M. I., Kemsley, J. N., Lee, S.-K., Lehnert, N., Neese, F., Skulan, A. J., Yang, Y.-S., and Zhou, J. (2000) *Chem. Rev.* **100,** 235–350
36. Clarkson, A. B., Jr., Bienen, E. J., Pollakis, G., and Grady, R. W. (1989) *J. Biol. Chem.* **264,** 17770–17776
37. Iwaki, M., Giotta, L., Akinsiku, A. O., Schägger, H., Fisher, N., Breton, J., and Rich, P. R. (2003) *Biochemistry* **42,** 11109–11119
38. Breton, J., and Nabedryk, E. (1996) *Biochim. Biophys. Acta* **1275,** 84–90
39. Iwaki, M., and Rich, P. R. (2004) *J. Am. Chem. Soc.* **126,** 2386–2389
40. Rich, P. R. (2004) *Biochim. Biophys. Acta* **1658,** 165–171
41. Koppenhöfer, A., Turner, K. L., Allen, J. W. A., Chapman, S. K., and Ferguson, S. J. (2000) *Biochemistry* **39,** 4243–4249
42. Voevodskaya, N., Narvaez, A.-J., Domkin, V., Torrents, E., Thelander, L., and Gräslund, A. (2006) *Proc. Natl. Acad. Sci. U.S.A.* **103,** 9850–9854
43. Atkin, C. L., Thelander, L., Reichard, P., and Lang, G. (1973) *J. Biol. Chem.* **248,** 7464–7472
44. Albury, M. S., Affourtit, C., Crichton, P. G., and Moore, A. L. (2002) *J. Biol. Chem.* **277,** 1190–1194
45. Moore, A. L., and Albury, M. S. (2008) *Biochem. Soc. Trans.* **36,** 1022–1026
46. Berthomieu, C., and Hienerwadel, R. (2005) *Biochim. Biophys. Acta* **1707,** 51–66
47. Berthomieu, C., Boullais, C., Neumann, J.-M., and Boussac, A. (1998) *Biochim. Biophys. Acta* **1365,** 112–116
48. Berthomieu, C., Hienerwadel, R., Boussac, A., Breton, J., and Diner, B. A. (1998) *Biochemistry* **37,** 10547–10554
49. Walden, S. E., and Wheeler, R. A. (1996) *J. Chem. Soc. Perkin Trans.* **2,** 2663–2672

Title:

Visualization of mitochondrial and apicoplast nucleoids in the human malaria parasite *Plasmodium falciparum* by SYBR Green I and PicoGreen staining

Authors:

Katsura SANO-MAEDA[1], Shigeharu SATO[2], Takashi UEDA[3], Ryoko YUI[4], Kie ITHO[4,5], Masayuki HATA[6], Akihiko NAKANO[3,7], Kiyoshi KITA[6], Kimiko MURAKAMI-MUROFUSHI[1], Narie SASAKI[4]*

Institutions:

[1]Department of Biology, Faculty of Science, Ochanomizu University, Tokyo 112-8610, Japan

[2]Division of Parasitology, MRC National Institute for Medical Research, London NW7 1AA, UK

[3]Department of Biological Sciences, Graduate School of Science, The University of Tokyo, Tokyo 113-0033, Japan

[4]Division of Biological Science, Graduate School of Science, Nagoya University, Nagoya 464-8602, Japan

[5]Department of Integrated Biosciences, Graduate School of Frontier Sciences, University of Tokyo, Kashiwa 277-8562, Japan

[6]Department of Biomedical Chemistry, Graduate School of Medicine, The University of Tokyo, Tokyo 113-0033, Japan

[7] RIKEN Advanced Science Institute, Saitama 351-0198, Japan

*Corresponding author

Narie Sasaki

E-mail: narie@bio.nagoya-u.ac.jp

Furo-cho, Chikusa-ku, Nagoya, Aichi 464-8602

Running title: Organellar nucleoids of the malaria parasite

Summary

Organellar DNA in mitochondria and plastids are organized with proteins into a compact structure known as the nucleoid. As the nucleoid is supposed to be the unit of inheritance for the organellar genome, it is important to understand its cytological behavior. Like plants, malaria parasites carry two organelles, the mitochondrion and the apicoplast - a non-photosynthetic plastid. However, probably because of the small size of the genome in each, visualizing the nucleoid in the *Plasmodium* organelles by regularly-used fluorescent dye such as DAPI has been difficult. Here, we developed new, effective methods to visualize the organellar nucleoid in the human malaria parasite *Plasmodium falciparum*. With our methods with SYBR Green I or PicoGreen, nucleoids were observed in ring-stage parasites. Analyzing transfectant parasites carrying a DsRed-labelled organelle, we concluded that the parasite's mitochondrion has one nucleoid which is visualized with our methods. The parasite has a second nucleoid in the apicoplast, but higher concentration of the dye was required to visualize it. Our new methods would be useful for further cytological analysis of the nucleoids in the mitochondrion and the apicoplast of the malaria parasite.

Key words: mitochondrial DNA (mtDNA), apicoplast DNA (apDNA), nucleoid, SYBR green I, PicoGreen, *Plasmodium falciparum*

Introduction

As like other apicomplexan parasites, the cell of malaria parasites (*Plasmodium* spp.) contains two extrachromosomal DNA (Wilson *et al.* 1994, Feagin 1994, Wilson and Williamson 1997). They are the genomic DNAs of the mitochondrion (mtDNA) and the secondary plastid called apicoplast (apDNA). Those genomes are smallest known organellar genome. Although mammalian mtDNA is a circular DNA with approximately 16 kbp (Wallace 1994), the mtDNA of the human malaria parasite *P. falciparum* is a mixture of linear oligomers of a unit of 6 kbp (Preiser *et al.* 1996). The 6 kbp unit encodes just three components of the parasites' electron transport chain, cytochrome *b* and subunits I and III of cytochrome *c* oxidase, and scrambled fragments of two ribosomal RNAs (Vaidya *et al.* 1989, 1993). Although the mitochondrion is not believed to be a site of ATP generation in malaria parasites (Fry *et al.* 1990), the mitochondrial electron transport chain is critical for parasite survival, and inhibition of cytochrome *b* is an antimalarial drug target (Biagini *et al.* 2008). Each ring-stage parasite cell carries a single mitochondrion with ~20 units of the 6 kbp mtDNA (Preiser *et al.* 1996).

On the other hand, the apDNA of *P. falciparum* is a 35 kbp circular molecule (Wilson *et al.* 1996). Almost all proteins encoded by the apDNA are involved in prokaryote-type transcription and translation, and some antibiotics affecting those prokaryotic functions cause the delayed-death phenotype of the parasites (Dahl and Rosenthal 2008). This fact suggests that at least one gene encoded by the apDNA should be critical for the parasite's survival. A *P. falciparum* cell at the ring stage carries a single apicoplast that seems to contain only one or a few copies of apDNA (Kohler *et al.* 1997, Williamson *et al.* 2002).

It has been known that the organellar DNA is packed with proteins into highly organized structures called nucleoids in a wide variety of organisms (Kuroiwa 1982, Sato *et al.* 2003). As the nucleoid is thought to be a unit of genetic inheritance of the organelle (Garrido *et al.* 2003, Jacobs *et al.* 2000), it is important to study its behaviors in the living cell. Usually, nucleoids are visualized by staining with a fluorescent DNA dye such as DAPI, and indeed, the presence of the nucleoid in both the mitochondrion and the apicoplast has been confirmed in an apicomplexan parasite *Toxoplasma gondii* stained with the dye (Matsuzaki *et al.* 2001). However, the nucleoid in *Plasmodium* has been detected only in the apicoplast as a weak signal when it was staining with DAPI or Hoechst33342 (Wilson *et al.* 1996, Stanway *et al.* 2009); any nucleoid-like body has never been identified in the parasite's mitochondrion.

In this study, we attempted to develop a reliable method to visualize both mitochondrial and apicoplast nucleoids in living *P. falciparum* cells using two highly sensitive fluorochromes, SYBR Green I and PicoGreen.

Material and Methods

Cell culture

The 3D7 strain of *Plasmodium falciparum* was cultured in vitro with human erythrocyte following the method described by Trager and Jensen (1976), with modifications. The culture was maintained with 3% hematocrit in RPMI 1640 medium (Invitrogen) supplemented with 10% (v/v) type A human serum.

Transfection

P. falciparum 3D7 was transfected with either pSSPF2/PfHsp60-DsRed, which expresses a mitochondrion-localizing DsRed, or pSSPF2/PfACP-DsRed, which express an apicoplast-localizing DsRed (Sato and Wilson 2004), by electroporation and each transfectant was selected following the method described in a previous report (Kobayashi *et al.* 2007).

DNA staining and microscopic observation

The SYBR Green I solution (Molecular Probes) was diluted to one of the several different concentrations with the cell culture medium as seen in text and the erythrocyte infected by the *P. falciparum* was incubated in the dye-containing medium for 1 minute, followed by microscopic observation under laser scanning microscopes, LSM700 (ZEISS; Fig. 1) or LSM710 (ZEISS; Fig. 2). The PicoGreen solution (Molecular Probes) was diluted in 1:300 or 1:1,000 (v/v) with the cell culture medium and the parasite was incubated in each dye-containing medium for 1 minute, 30 minutes or 1 hour under the standard culture conditions, followed by microscopic observation using one of the microscopy systems mentioned above.